A STUDY ON MATHEMATICAL MODELING OF DIRECT SYNTHESIS OF DIMETHYL ETHER IN STRUCTURED MEMBRANE REACTORS

by

Hayrettin Hasan Köybaşı

B.S., Chemical Engineering, Boğaziçi University, 2019

Submitted to the Institute for Graduate Studies in
Science and Engineering in partial fulfillment of
the requirements for the degree of
Master of Science

Graduate Program in Chemical Engineering

Boğaziçi University

2022

ACKNOWLEDGEMENTS

First and foremost, I would like to express my deepest appreciation and gratitude to my thesis supervisor Prof. Avci, who has been extremely supportive and attentive during my studies. His knowledge and guidance has been transformative and invaluable in my pursuit of knowledge in chemical engineering.

Apart from my advisor, I would like to thank Assoc. Prof. A. Kerem Uğuz and Prof. Seda Keskin for devoting their precious time to evaluate my research. Their insights and encouragement are very much appreciated.

My ambition and curiosity in chemical engineering is mostly due to excellent faculty members in our department. I would like to thank every single professor and teaching assistant who took part in my education.

Special thanks to Ceren Hatipoğlu for her collaboration and contribution in our joint projects. My former colleagues Selin Baç Bilgi and Sinan Koç shared alot of their technical knowledge with me which I can not appreciate enough. Additionally, I would like to thank my friends from KB 404; Necdet Semih Altınsoy, Mert Özden, Mertcan İnce and Özge Selçuk. I would like to thank my former classmate and fellow teaching assistant Enes Emre Taş for his support and friendship throughout many years.

I would like to thank my family for their continous love and support. My sister helped me greatly in becoming who I am and I appreciate her support dearly.

Finally, I acknowledge the financial support provided by TÜBİTAK project no: 118M518.

ABSTRACT

A STUDY ON MATHEMATICAL MODELING OF DIRECT SYNTHESIS OF DIMETHYL ETHER IN STRUCTURED MEMBRANE REACTORS

Catalytic transformation of CO_2 into dimethyl ether (DME) is modeled in a membrane microchannel reactor. The reactor geometry includes an α-Al_2O_3 supported SOD membrane layer, capable of *in-situ* H_2O removal, residing between a reaction channel and a parallel permeate channel. Reaction channels are washcoated with a physical mixture of Cu–ZnO/Al_2O_3 (CZA) and HZSM–5 catalysts, which are responsible for the synthesis and dehydration of methanol respectively. CO_2-H_2 reactant mixture (H_2/CO_2=3) is dosed to the reaction channel at space velocity=6×10^3 ml $gcat^{-1}$ h^{-1} whereas, pure H_2 at identical temperature and pressure, is fed to the permeate channel to sweep permeated steam. A steady-state isothermal reactor model based on the mass and momentum conservation equations is solved numerically using ANSYS software. Computed performance metrics show minimal deviation from the reported experimental data at 483–543 K, 30–50 bar. Incorporation of energy conservation to the model results in near-constant temperature profile and almost identical reactor performance, which validates isothermal operation. Owing to steam efflux from and H_2 influx to the reactive stream, membrane integration increases CO_2 conversion ($\sim$ 60%) and DME yield ($\sim$ 30%) by a factor of >3 compared to membraneless operation. The benefits become more significant at higher temperature and pressures. Sending sweep H_2 counter-currently offers superior H_2O removal. Relative inlet velocity of the permeate inlet (v_{rat}) affects membrane mass transfer dramatically. Adopting higher CZA/HZSM-5 mass ratio improves both performance metrics and the reactor capacity. With a $\sim$7 m^3 reactor system, 2.76×10^2 tons of DME can be synthesized from 1×10^3 tons of CO_2 annually, provided that 1 MW electrolyzer provides the required H_2.

ÖZET

MİMARİLİ MEMBRAN REAKTÖRLERDE DİMETİL ETER SENTEZİNİN MATEMATİKSEL MODELLENMESİ

CO_2'nin dimetil etere (DME) katalitik dönüşümü membranlı mikrokanal reaktörde modellenmiştir. Buharı ayrıştırabilen α-Al_2O_3 destekli SOD membran tabakası, reaktör mimarisinde reaksiyon ve süpürme kanalları arasında bulunmaktadır. Reaksiyon kanalları, sırasıyla metanolün oluşumu ve dehidrasyonundan sorumlu Cu–ZnO/Al_2O_3 (CZA) ve HZSM–5 katalizörlerinin fiziksel karışımıyla kaplanmıştır. CO_2-H_2 gaz karışımı (H_2/CO_2=3) reaksiyon kanalına 6×10^3 ml g_k^{-1} sa^{-1} boşluk hızıyla gönderilmiş, eşit sıcaklık ve basınçtaki H_2 gazı ise membrandan süzülen buharı uzaklaştırmak üzere süpürme kanalına beslenmiştir. Kütle ve momentum korunum denklemlerini baz alan izotermal yatışkın hal modeli ANSYS programında numerik olarak çözülmüştür. Hesaplanan performans metrikleri, 483–543 K ve 30–50 bar aralığında literatürde belirtilen deneysel verilerden minimal sapma göstermektedir. Enerji korunum denklemlerinin modele eklenmesiyle elde edilen neredeyse sabit sıcaklık profili ve değişmeyen reaktör performansı, izotermal koşulların geçerliliğini tasdik etmektedir. Membran entegrasyonu reaksiyon karışımına H_2 girişi ve H_2O çıkışı sağladığından, CO_2 dönüşümünü ($\sim$ %60) ve DME verimini ($\sim$ %30) membransız sonuçlara göre en az üç kat artırmaktadır. Sıcaklık ve basıncın artırılması membran işlevini ve faydalarını daha belirgin hale getirmektedir. Süpürücü H_2 gazını zıt yönlü beslemek daha üstün H_2O ayrımı sağlamaktadır. Süpürme kanalının oransal giriş hızı (v_{rat}) membran kütle aktarımını önemli ölçüde etkilemektedir. Katalizör kütle oranını (CZA/HZSM-5) artırmak hem performans metriklerini hem de reaktör kapasitesini iyileştirmektedir. 1 MW'lık elektrolizörün gerekli hidrojeni sağlaması halinde, $\sim$7 m^3'lük reaktör sistemi yıllık 1×10^3 ton CO_2'den 2.76×10^2 ton DME sentezleyebilmektedir.

TABLE OF CONTENTS

LIST OF FIGURES

LIST OF TABLES

LIST OF SYMBOLS

C_2	Inertial resistance coefficient of the washcoat, m^{-1}
$c_{p,i}$	Heat capacity of species *i*, J kg^{-1} K^{-1}
$c_{p,m}$	Heat capacity of gas mixture, J kg^{-1} K^{-1}
$D_{eff,i,m}$	Effective diffusivity of species *i* in the mixture, m^2 s^{-1}
$D_{i,j}$	Binary diffusion coefficient, m^2 s^{-1}
$D_{i,m}$	Diffusion coefficient of species *i* in the mixture, m^2 s^{-1}
$D_{K,i}$	Knudsen diffusivity of species *i*, m^2 s^{-1}
d_p	Particle diameter (equalized to the thickness of the catalyst washcoat layer), m
d_{pore}	Average pore diameter, m
f_i	fugacity of species *i* in the mixture, bar
F_i	Molar flow rate of the component *i*, mol s^{-1}
$f_{pure,i}$	Fugacity of pure species *i*, bar
$f_{pure,i}$	Fugacity of pure species *i*, bar
$G_{f,i}$	Gibbs free energy of formation of species *i*, kJ mol^{-1}
$H_{f,i}$	Enthalpy of formation of species *i*, kJ mol^{-1}
H	Height of the microchannel, m
I	3x3 identity matrix
$\vec{J}_i$	Molar flux of species *i* through the membrane, mol m^{-2} s^{-1}
k_{cat}	Thermal conductivity of the catalyst layer, W m^{-1} K^{-1}
$K_{D,rxn}$	Reaction equilibrium constant, bar^{-2} (rxn=1, 3), – (rxn=2,4)
$k_{eff,m}$	Effective thermal conductivity of gas mixture in the washcoat layer, W m^{-1} K^{-1}
K_i,K'_i	Adsorption/desorption equilibrium constant for species *i*, bar^{-1}
k_i	Thermal conductivity of species *i*, W m^{-1} K^{-1}
k_m	Thermal conductivity of gas mixture, W m^{-1} K^{-1}

k_{rxn}	Reaction rate constant, mol g_{cat} s^{-1} $bar^{-1.5}$ for rxn=1, 3; mol g_{cat} s^{-1} bar^{-1} for rxn=2; mol g_{cat} s^{-1} bar^{-2} for rxn=4
k_w	Thermal conductivity of the membrane layer, W m^{-1} K^{-1}
L	Length of the microchannel, m
l_{edge}	Edge length of a mesh cell, m
M_i	Molecular weight of species i, kg mol^{-1}
M_m	Average molecular weight of gas mixture, kg mol^{-1}
n_i	Number of moles of species i, mol
N_g	Number of gas phase species i, –
p	Total pressure, bar
$p^i{}_{perm}$	Partial pressure of species i in the permeate channel, Pa
$p^i{}_{rxn}$	Partial pressure of species i in the reaction channel, Pa
$Perm_i$	Membrane permeability of species i, mol m^{-2} s^{-1} Pa^{-1}
R	Gas constant (=8.314 J mol^{-1} K^{-1})
R_i	Consumption/generation rate of species i, mol m^{-3} s^{-1}
r_{rxn}	Rate of a reaction, kmol m^{-3} s^{-1}
S_i	Mass source term of species i, kg m^{-3} s
$S_{f,i}$	Entropy of formation of species i, kJ mol^{-1}, K^{-1}
T	Temperature, K
v_{rat}	Ratio of permeate inlet velocity to the fixed reactive stream inlet velocity, –
$\vec{v}$	Velocity vector, m s^{-1}
W	Width of the microchannel, m
x, y, z	Cartesian coordinates
X_{CO_2}	CO_2 conversion (defined in Equation (**??**))
Y_{DME}	DME yield (defined in Equation (**??**))
Y_i	Mass fraction of species i, –
y_i	Mole fraction of species i, –
Z	Compressibility factor of gas mixture, –

ΔG_{rxn}	Gibbs free energy of reaction, kJ mol^{-1}
ΔH^{o}	Standard enthalpy of reaction, kJ mol^{-1}
ΔH_{rxn}	Heat of reaction, kJ mol^{-1}
ε_{cat}	Porosity of the washcoat layer, –
$\Phi_{i,j}$	Dimensionless parameter for the mixture of i and j, –
μ_i	Viscosity of species i, kg m^{-1} s^{1}
μ_m	Average gas mixture viscosity, kg m^{-1} s^{1}
ρ_m	Density of gas mixture, kg m^{-3}
ρ_{cat}	Density of the catalyst mixture, kg m^{-3}
ρ_{CZA}	Density of Cu-ZnO-Al_2O_3, kg m^{-3}
$\rho_{CZA,mix}$	Density of CZA catalyst in the catalyst layer, kg m^{-3}
ρ_{HZSM-5}	Density of HZSM−5 catalyst, kg m^{-3}
$\rho_{HZSM-5,mix}$	Density of HZSM−5 in the catalyst layer, kg m^{-3}
$\left(\sum v\right)_i$	Sum of the atomic diffusion volumes for species i, –
τ_{cat}	Catalyst tortuosity, –

LIST OF ACRONYMS/ABBREVIATIONS

1D	One Dimensional
2D	Two Dimensional
3D	Three Dimensional
CH_3OH	Methanol
CH_3OCH_3	Dimethyl ether
CH_4	Methane
CO	Carbon monoxide
CO_2	Carbon dioxide
CO_2	Carbon dioxide
CP	Porous catalyst phase
CZA	Cu-ZnO/Al_2O_3
DME	Dimethyl ether
FP	Fluid phase
H_2	Hydrogen
H_2O	Water
HZSM-5	Zeolite socony mobil no. 5
MW	Molecular weight
NO_x	Nitrogen oxides
RWGS	Reverse water-gas shift reaction

1. INTRODUCTION

Significant increase in global average temperatures driven by accumulation greenhouse gases such as CH_4 and CO_2 in the atmosphere, has the potential to cause major economic and environmental devastation. Countries around the world have pledged to reduce their CO_2 emissions by increasing the share of renewable sources in their power grids. The strong motivation in gradual replacement of fossil-fuel based conventional energy infrastructure, drives significant interest in sustainable energy technologies.

Sunlight can be converted directly into renewable energy by photovoltaic systems. Alternatively, indirect transformation of solar energy can be accomplished by wind and hydropower. Renewable energy can also be used in the production of so-called "green hydrogen". Challenges associated with H_2 storage and handling can be addressed by its subsequent transformation into ammonia, methane, methanol or dimethyl ether [1].

Carbon capture and utilization technologies (CCU) not only offer sustainable methods to synthesize useful chemicals but they have the capability to utilize atmospheric CO_2 as the carbon source. CO_2 can be used as feedstock to synthesize various chemicals such as carbamic acids, polycarbonates, dimethyl carbonate, methanol and dimethyl ether [2]. Since the majority of fossil fuels are extracted to power transportation and energy generation, synthesis of alternative fuels from CO_2 offers a major opportunity in sustainable future. Such a scenario would create a circular carbon economy where new oil and natural gas discoveries become redundant.

Dimethyl ether (DME) is a volatile organic compound with the formula CH_3OCH_3. It is transformed into liquid phase at pressures above 5 bar. DME shares similar characteristics with butane and propane, and it burns with visible blue flame. Molecular structure of DME is composed of C-O and C-H bonds, while lacking any C-C bond. It is considered as an extremely promising alternative fuel due to its ease of transportation and handling, non-toxicity, high cetane number, smokeless combustion and low combustion noise.

DME can be used in conventional compression-ignition engines, provided that fuel injection equipment is modified slightly for such application. On the other hand, its corrosiveness, low combustion enthalpy, low density/lubricity pose a challenge for its mainstream adoption [3]. In addition to being a potential fuel source, DME can also be used as a feedstock to synthesize various chemicals like dimethyl sulfate, methyl acetate and light olefins [4].

Table 1.1. Physical properties of dimethyl ether [5].

Molecular formula	C_2H_6O
Molar mass	46.07 g mol^{-1}
Appearance	Colorless gas
Liquid density	667 kg m^{-3}
Melting point	-141 ^{o}C, 132 K
Boiling point	-24 ^{o}C, 249 K
Solubility in water	71 g dm^{-3} at (20 ^{o}C)
Vapor pressure	>100 kPa
Auto-ignition point	235^{o}C, 508 K

Conventional DME synthesis is based on so-called indirect route, where methanol synthesis and dehyration reactions take place in separate reactors. Synthesis gas, a mixture of carbon oxides (CO + CO_2) and hydrogen (H_2), is transformed into methanol in the first reactor via metallic catalysts. Following the purification steps, methanol is dehydrated into DME in a second reactor containing solid acid catalyst. In an alternative approach called direct route, methanol synthesis and dehydration steps can be combined in a single reactor. Either bi-functional catalysts or physical mixtures of acidic and metallic catalysts can be used for this purpose. Direct route offers some advantages over the indirect approach. Since fewer reactors need to be installed, required capital investment is lower. Moreover, since methanol is converted and removed from the reactive mixture, thermodynamic limitations on methanol synthesis are minimized [5].

Due to exothermic nature of hydrogenation and dehydration reactions, temperature regulation plays a key role in DME synthesis. Catalyst deactivation and undesired side reactions become more significant at elevated temperatures. In addition, at higher temperatures, lower equilibrium conversions can be achieved. The requirement for facile temperature regulation is more relavant for the direct route, since combination of exothermic reactions lead to faster rate of heat generation. Temperature variation within reactor can reach up to ~40 K when cooling-integrated fixed bed reactor is used. On the other hand, near isothermal conditions can be obtained with microchannel reactors. Volumetric intensification results in transport rates up to two orders of magnitude larger than those obtained with fixed bed reactors. A typical microchannel reactor involves parallel channels having dimensions between 10^{-6} and 10^{-3} m. Hence, compared to conventional packed bed geometries, surface area to volume ratio of microchannel reactors is $\sim 10^3$ times higher. Additionally, the capacity of microchannel system can be varied easily by changing the number of microchannels [6].

Sourcing syngas from sustainable feedstocks such as biomass is a promising approach in DME synthesis. On the other hand, biomass-derived syngas has signifcantly higher CO_2 content compared to syngas derived from steam reforming [7]. Presence of CO_2 in the reaction mixture creates several undesired effects. High CO_2 partial pressures lead accelerated RWGS reaction and subsequent steam generation. Being a side product of DME synthesis, accumulation of steam suppresses the rate of methanol dehydration thermodynamically. Furthermore, hydrothermal sintering of catalyst become more pronounced with high steam concentrations. Unless H_2O in the reaction media is removed effectively, DME synthesis via CO_2 hydrogenation becomes impractical [8].

Several strategies can be adopted to avoid negative consequences of steam accumulation via selective *in-situ* steam removal [9]. Sorption-enhanced DME synthesis involves packing H_2O selective sorbent materials alongside catalyst particles. Due their small micropores blocking large molecules, zeolite materials such as 3A and 4A, offers high affinity and selectivity towards steam. On the other hand, since sorbent materials become saturated with H_2O as time progresses, adsorbent needs to be regenerated by the removal of adsorbed H_2O. *In-situ* H_2O removal can also be accomplished by the use of steam-selective membranes.

Unlike sorption enhanced process, adsorption-desorption cycles are not needed, hence, continuous operation is possible. Several membrane materials such as ZSM-5, MOR, sodalites and polymer nafion are propsoed for steam removal applications. Among them, sodalite (SOD) materials offer moderate H_2O permeance and excellent permselectivity, preventing cross membrane transfer of CO_2, CH_3OH, CH_3OCH_3. Relatively low H_2O/H_2 permselectivity of SOD membranes leads to another key benefit. The rate of methanol formation can be improved significantly by keeping high H_2 content in the reaction mixture via cross membrane H_2 transport [10]. For this purpose, H_2 can be selected as sweep gas to maximize H_2 concentration on the permeate side.

Integrating membranes to microchannel reactors combines the benefits of both volumetric and functional intensification. High surface area of microchannel reactors provides extended contact between fluids and membrane surface. Furthermore, temperature and flow rate of sweep gas can be easily manipulated to accomplish effective temperature regulation. Remarkable improvements in CO_2 conversion and DME yield are reported upon adopting membrane-integrated micro-structured systems [11, 12]. It should be noted that, these studies involve CO_2 containing syngas as feedstock. On the other hand, CO_2 derived from air separation or carbon capture can also be used to synthesize DME. Moreover, clean H_2 derived from renewable energy can be selected as the second raw material. Such an approach can lead to carbon neutral fuel production where solar energy is stored in DME molecule as chemical energy.

This thesis is composed of five main chapters, including Introduction. Detailed literature survey about DME synthesis and associated process intensification are presented in Chapter 2. Details about the reactor geometry and operating parameters, reaction network and kinetic model, membrane model and solution methodology is given in Chapter 3. In Chapter 4, reactor model and isothermal conditions are validated in the first two sections. Then, detailed discussion about the results of the parametric study is provided. Key conclusions obtained from this work and recommendations are provided in Chapter 5.

2. LITERATURE SURVEY

2.1. Dimethyl Ether Production

Syngas, a mixture of carbon oxides and hydrogen, derived mainly from hydrocarbons via reforming or gacification reactions, is used to synthesize DME. Catalytic reactions taking place in the synthesis [5, 13] can be listed as

$$CO_2 + 3\,H_2 \rightleftharpoons CH_3OH + H_2O \qquad \Delta H^o = -49.4\text{kJ mol}^{-1} \qquad (2.1)$$

$$CO_2 + H_2 \rightleftharpoons CO + H_2O \qquad \Delta H^o = 41.0\text{kJ mol}^{-1} \qquad (2.2)$$

$$CO + 2\,H_2 \rightleftharpoons CH_3OH \qquad \Delta H^o = -90.4\text{kJ mol}^{-1} \qquad (2.3)$$

$$2\,CH_3OH \rightleftharpoons CH_3OCH_3 + H_2O \qquad \Delta H^o = -23.0\text{kJ mol}^{-1}. \qquad (2.4)$$

Due to exothermic nature of methanol formation and DME synthesis reactions, unless effective cooling is applied, temperature of the reaction mixture increases. Such a situation may increase temperature above 573 K, resulting in undesired methanation reaction which can be expressed as

$$CO + 3\,H_2 \rightleftharpoons CH_4 + H_2O. \qquad (2.5)$$

Currently, DME production can take place with two different approaches. The first one which is called two-step or indirect route, methanol synthesis (Reactions (2.1) and (2.3)) and methanol dehydration (Reaction (2.4)) occur in two separate reactors involving metallic and acidic catalysts, respectively. On the other hand, synthesis and dehydration of methanol take place in a single reactor simultaneously in the one-step or direct route. Combination of metallic and acidic functions is needed by using either bi-functional catalyst or a physical mixture of metallic and acidic catalysts. [5]. Key information derived from computational and experimental studies on both routes are presented in the following sections.

2.1.1. Indirect DME Production

Due to ease of product purification and high DME selectivity obtained at mild conditions, conventional DME synthesis involves two-step process. Properties of different dehydration catalysts is the main focus of studies involving two step synthesis. Operating temperature is typically varied within 380-720 K. On the other hand, due to reaction stoichiometry of Reaction (4), the effect of pressure has lower impact.

Additional parameters such as pressure, H_2/CO ratio, effect of co-feeding CO_2 and space velocity are also investigated at operating condtions of 1-100 bar, 0.5-2.5 and 00-3000 h^{-1} [14]. In these studies, CO conversion and DME yield are typically between 20-97% and 10-100% respectively. Apart from traditionally adopted fixed bed reactor, indirect route is also investigated for reactive distillation [15], catalytic membrane reactor [16] and Platelet Milli-reactor [17]. Furthermore, various solid acid catalyst such as γ-Al_2O_3 [18–20], HZSM-5 [21, 22], HY zeolite supported by modified Cu-Mn-Zn [23], mordenite [24], and Nafion [25] are tested in the synthesis of DME from methanol. Kinetic expressions in the form of Langmuir-Hinshelwood [26] and Eley-Rideal [27] mechanisms are derived for DME synthesis from methanol. These studies commonly point out that the presence of H_2O or DME slows the kinetics of Reaction (2.4) [15].

It is reported that 80% methanol conversion with no side product can be obtained above 573 K, when alumina impregnated SBA-15 (Al@SBA-15) catalyst is used in DME synthesis [25]. However, lower temperatures resulted in formaldehyde formation, with a yield of 20 % at 473 K. DME synthesis in a fixed bed reactor containing both γ-Al_2O_3 and HZSM-5 catalysts yielded higher activity than using γ-Al_2O_3 alone [28]. Additionally, stability of HZSM-5 is improved below 508 K. Production rate of 13.5 g_{DME} g_{cat}^{-1} h^{-1} is observed at 508 K. A study conducted by Chen *et al.* [14] revealed that, co-feeding CO_2 enhances CO conversion. At CO_2/CO=2, H_2/CO=4, 473 K optimum reactor performance is achieved where 90% CO conversion is observed. Zhu *et al.* [29] created a two stage reaction system where Cu-ZnO-Al_2O_3 and HZSM-5 catalyst are stacked consecutively.

Optimal operating temperatures of methanol synthesis and dehydration stages are found as 543-553 and 508-518 K, respectively. Selecting $H_2/CO>2$ greatly enhances reactor performance. CO conversion increases from 10% to up to 52% whereas, the change in DME yield is from 10% to 52%. Increasing pressure to 80 bar boosted reactor performance where 78% CO conversion and 63% DME yield obtained compared to 30% and 21 % at 30 bar, respectively.

2.1.2. Direct DME Production and Process Intensification

Direct DME synthesis require bi-functional or hybrid catalyst which combine metallic function catalyzing methanol synthesis and acidic character dehydrating dehydrating methanol into DME. Consumption and removal of methanol from the reaction environment relaxes thermodynamic limitations on methanol synthesis process, leading to higher CO conversions. Due to reduction in the number of reactors, required capital investment is relatively lower in the direct route.

Catalytic investigations for the direct route generally focus on optimizing CO conversion and DME yield by varying the dehydration catalyst and its degree of acidity. Solid acid catalysts like γ-Al_2O_3 [30–32], SiO_2-Al_2O_3 [33, 34] and zeolites like HZSM-5 H-Y, H-Beta and H-Ferrierite [35–37] are studied. At operating conditions of 513-553 K, 1-70 bar, H_2/CO=0.5-2, residence time=3-8 kg_{cat} h $kmol^{-1}$, CO conversions vary between 53% and 95%, and DME yield is in the range of 34-52%. In these studies, effect of Cu-ZnO/Al_2O_3 mass ratio is also investigated, by varying this parameter between 1:1 and 3:1. CO_2 can exist in synthesis gas in varying degrees based on the the production method. Certain studies focused on the impact of using CO_2 on direct DME synthesis at operating conditions of 513-543 K, H_2/CO_2=2-10 and 30-40 bar, resulting in 15-50% CO_2 conversions and 9-25% DME yields. Catalysts used in these studies are γ-Al_2O_3 [38], ZSM-5 [39] and HZSM-5 [40, 41]. Additional details on dehydration catalysts, and information related to the synthesis and characterization can be found in [13].

Apart from the properties of adopted catalysts, temperature regulation also plays a key role in direct DME synthesis. Due to exothermic reactions involved, equilibrium conversions decrease at elevated temperatures, which indicates potential drawbacks in the absence of a cooling system. At elevated temperatures, rate of Reaction (2) increases dramatically if CO_2 is present in the feed. Generated H_2O suppresses methanol dehydration and exacerbates hydrothermal sintering of both methanol synthesis and dehydration catalysts [13, 31, 42]. Furthermore, Reaction (2.2) also consumes H_2, whose partial pressure needs to be high to achieve satisfactory CO conversion. Therefore, CO_2 utilization via DME synthesis poses significant challenges.

Despite the strong correlation between the rate of heat removal from the catalyst bed and the reactor geometry, studies concerned about this aspect are limited. A microchannel reactor packed with a physical mixture of F51-8PPT (methanol syntheis) and ZSM-5 (methanol dehydration) catalysts, is investigated by Hu *et al.* [43]. Volumetric miniaturization and subsequent facile temperature regulation, improved DME yield three-folds and prevented catalyst deactivation. Hayer *et al.* performed both experimental and computational studies involving heat-exchange integrated microchannel reactor, packed with metallic (CZA) and solid acid (γ-Al_2O_3 and HZSM-5) catalysts [44–46]. Effects of temperature and pressure, feeding rate, stream composition and coolant inlet temperature on CO conversion and DME selectivity is investigated. Cooling integration and volumetric miniaturization enabled significant intensification of direct DME synthesis. McBride *et al.* compared layered and and physical mixture arrangements of methanol synthesis and dehydration catalysts. A significant increase in DME productivity is observed when physical mixture is adopted over layered configuration. Catalysts can be incorporated into microchannel reactors by either packing them in particulate form or coating microchannels with a thin layer of catalyst. The latter strategy proved to be superior for various reaction systems [47, 48]. Wall-coated microchannel reactors offers heat transfer rates $\sim 10^2$ higher compared to configurations involving packed particulate catalysts. Furthermore, transport resistances can be minimized and near ideal catalyst effectiveness can be observed [49–52]. A typical high-performance microchannel reactor involves washcoated channels with hydraulic diameters within 10^{-6}-10^{-2} m.

They are generally created from metallic substrates via micromachining techniques, having surface area-to-volume ratios up to 10^4 m^2 m^{-3}. Combined with their high transport rates, microchannel reactors enables near-isothermal operation [53, 54].

Functional intensification of DME synthesis via *in-situ* steam removal is also extremely promising. In a conventional DME synthesis, steam generated from Reaction (2.4) is consumed by water gas shift reaction, leading to thermodynamic synergy between reactions. Furthermore, H_2 is generated, which improves the rate of methanol synthesis. However, CO_2 is also produced as a side product, leading to problematic CO_2 emissions [8]. One-step DME synthesis via CO_2 hydrogenation suffers from significant thermodynamic limitations. Steam generated via Reactions (2.1-2.2 and 2.4) accumulates within the reaction media and hinders both methanol formation and dehydration rections [55]. Removal of H_2O from the reaction media relaxes the thermodynamic limitations and allow CO_2 to be used as a feedstock in DME synthesis. Several studies [56–58] investigated incorporation of steam-selective adsorbents alongside catalyst particles. In this so-called sorption enhanced DME synthesis, equilibrium CO_2 conversion and yield is easily surpassed. For the sorption process, typically, 3A, LTA zeolites are selected [9]. In an alternative approach, *in-situ* steam removal can also be accomplished via steam-selective membranes. Iliuta *et al.* [8] created one-dimensional isothermal unsteady state model to investigate direct DME synthesis in a membrane reactor containing CZA and HZSM-5 mixture. Superior DME yield and selectivity are obtained in the presence of a steam-selective membrane. Diban *et al.* [55] created a one-dimensional isothermal model to simulate lab-scale membrane reactor. Influence of H_2O permeance and H_2O permselectivity on reactor performance is elucidated. De Falco *et al.* [59] simulated an industrial scale fixed bed reactor surrounded by hydrophilic ZSM-5 membrane. Remarkable improvements in CO_2 conversion and DME yield are observed compared to conventional reactor without a membrane.

This study aims to investigate direct DME synthesis in a membrane microchannel reactor. Unlike similar studies, Pure CO_2 derived from air separation or carbon capture, and H_2 produced via water electrolysis will be considered to be the feedstock of the reactor system.

A detailed two-dimensional mathematical model will be created to study the effects of various operating parameters on CO_2 conversion and DME yield. In addition. Validity of the mathematical model and isothermal operation will be tested. Finally a pilot scale reactor scheme will be sized based on H_2 production rate of a 1 MW water electrolyzer powered by renewable energy.

3. MATHEMATICAL MODELING

3.1. Details of the Multifunctional Reactor

A simplified illustration of the membrane microchannel reactor system is presented in Figure 3.1. Rectangular reaction and permeate channels with identical dimensions of 1.5×10^{-1} m (L), 3×10^{-4} m (H), and 6×10^{-4} (W) m, are separated with 1×10^{-3} m thick α-Al_2O_3 supported SOD membrane layer. Unlike permeate channel, reaction channel is washcoated with 5×10^{-5} m thick catalyst layer which contains a physical mixture of Cu-ZnO-Al_2O_3 and HZSM-5. Rectangular cross-section is adopted since conventional micromachining techniques are more suitable to create such structures [60], whereas channel dimensions are selected considering the balance between pressure drop and transport rates [61]. The design is coherent with a previous work involving a microchannel reactor containing a membrane and washcoated catalyst layer [62].

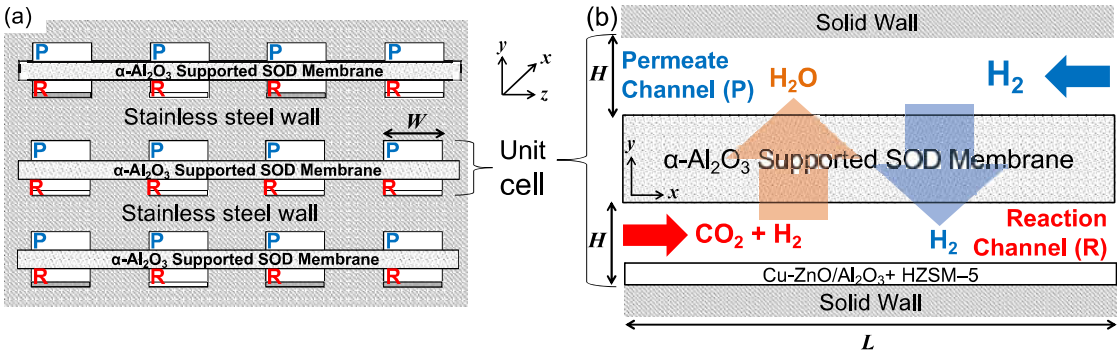

Figure 3.1. Simplified (not to scale) drawings of a multi-functional reactor block (left) and repeating unit cell (right).

Operating range of the reactor is determined based on the study of An *et al.* [63], which involves experimental investigation of DME synthesis via CO_2 hydrogenation. In this regard, a mixture of CO_2 and H_2 (H_2/CO_2=3) is dosed to the reaction channel with a space velocity of 6×10^3 ml g_{cat} h^{-1}.

Based on the assumption of green H_2 via electrolysis of water driven by renewable (i.e. solar and/or wind generated) electricity [64], pure H_2 is fed to the permeate channel, which sweeps permeated H_2O and a portion of it mixes with the reactive flow via cross-membrane transport. Such a H_2 feeding strategy resulted in superior reactor performances in previous studies [11, 12]. Inlet velocity magnitudes of the reaction and permeate channels are determined as 2.2×10^{-3} and 2.2×10^{-2} m s^{-1} respectively, based on adopted space velocity and v_{rat} (Ratio of permeate inlet velocity to the fixed reactive stream inlet velocity) at default operation. Inlet temperature and pressure of both channels are kept identical, which are 523 K, 50 bar at default operation. A parametric study is conducted by varying a selected parameter within the range given in Table 3.1, and other parameters are kept at their default values.

Table 3.1. Operating parameters of the microchannel reactor system.

Parameter	**Default value**	**Range**
Temperature at the reaction channel inlet (K)	523	503–543
Pressure at the reaction channel inlet (bar)	50	30–50
Temperature at the permeate channel inlet (K)	Same as the reaction channel inlet	
Pressure at the permeate channel inlet (bar)	Same as the reaction channel inlet	
Molar inlet H_2/CO_2 ratio	3	1–4
Reaction channel inlet velocity (m s^{-1})	2.2×10^{-3}	-
Space velocity (ratio of the volumetric flow rate of reactants to the mass of catalyst) (ml g_{cat}^{-1} h^{-1})	6×10^{3}	-
Ratio of the permeate channel inlet velocity to the reaction channel inlet velocity (v_{rat})	10	5–20
Mass ratio (CZA/HZSM–5) of catalysts	2	1–3
Relative flow direction	Counter–current	Co/counter–current

Reactor performance is measured by fractional CO_2 conversion and DME yield, whose respective definitions are given as [63]

$$CO_2\ conversion\ (X_{CO_2}) = (F_{in,CO_2} - F_{out,CO_2})/(F_{in,CO_2}) \tag{3.1}$$

$$DME\ yield\ (Y_{DME}) = 2 \times F_{out,DME}/(F_{in,CO_2}) \tag{3.2}$$

It should be noted that, cross-sectional surface averaged molar flow rates of the associated species are considered.

3.2. Reaction Network and the Kinetic Model

Physical mixture of Cu-ZnO-Al_2O_3 and HZSM-5 catalysts situated within the porous catalyst layer is responsible for the transformation of CO_2 into DME. Reactions (2.1-2.3) are driven by Cu-ZnO-Al_2O_3, whereas HZSM-5 catalyzes Reaction (2.4). Effect of methanation reaction and hydrothermal sintering of Cu-ZnO-Al_2O_3 catalyst are not considered in the model considering their negligible effect below 573 K [30]. Additionally, HZSM-5 exhibits excellent hydrothermal stability up to 773 K [65]. High CO_2 inlet concentration promotes reverse Boudouard reaction (2CO = CO_2 +C(s), ΔH^o= -172 kJ mol^{-1}), and prevents formation of carbon species [38, 42]. Based on these considerations, catalyst deactivation is neglected in the simulations. Kinetic expressions postulated by [65, 66] are adopted to the reactor model as

$$r_{rxn=(2.1)} = \frac{k_{rxn}K_{CO_2}\left[f_{CO_2}{f_{H_2}}^{3/2} - f_{CH_3OH}f_{H_2O}/({f_{H_2}}^{3/2}K_{D,rxn})\right]}{DEN = (1 + K_{\mathrm{CO}}f_{\mathrm{CO}} + K_{\mathrm{CO_2}}f_{\mathrm{CO_2}})\left[{f_{H_2}}^{1/2} + (K_{H_2O}/{K_{H_2}}^{1/2})f_{\mathrm{H_2O}}\right]} \tag{3.3}$$

$$r_{rxn=(2.2)} = k_{rxn}K_{CO_2}\left(f_{CO_2}f_{H_2} - f_{H_2O}f_{CO}/K_{D,rxn}\right)/DEN \tag{3.4}$$

$$r_{rxn=(2.3)} = k_{rxn}K_{CO}\left(f_{CO}{f_{H_2}}^{3/2} - f_{CH_3OH}/({f_{H_2}}^{1/2}K_{D,rxn})\right)/DEN \tag{3.5}$$

$$r_{rxn=(2.4)} = \frac{k_{rxn}\left({f^2}_{CH_3OH} - f_{CH_3OCH_3}f_{H_2O}/K_{D,rxn}\right)}{1 + {K'}_{H_2O}f_{H_2O} + K_{CH_3OH}f_{CH_3OH}}. \tag{3.6}$$

Presented kinetic expressions require estimation of reaction equilibrium constants, which can be computed via the Gibbs free energy of the pertinent reaction as

$$K_{D,rxn} = exp(-\Delta G_{rxn}/RT). \tag{3.7}$$

Formation enthalpy and entropy of the reactive species are computed as a function of temperature, leading to Gibbs free energy of formation of species. Pertinent calculation steps can be showed as

$$\frac{H_{f,i}}{RT} = a_1 + a_2\frac{T}{2} + a_3\frac{T^2}{3} + a_4\frac{T^3}{4} + a_5\frac{T^4}{5} + \frac{b_1}{T} \tag{3.8}$$

$$\frac{S_{f,i}}{R} = a_1 + a_2\frac{T}{2} + a_3\frac{T^2}{3} + a_4\frac{T^3}{4} + a_5\frac{T^4}{5} + \frac{b_2}{T} \tag{3.9}$$

$$\frac{G_{f,i}}{RT} = \frac{H_{f,i}}{RT} - \frac{S_{f,i}}{R}. \tag{3.10}$$

Then, using reaction stoichiometry, Gibbs free energy of a reaction is obtained as

$$\Delta G_{rxn} = \sum_{i=products} n_i G_{f,i} - \sum_{i=reactants} n_i G_{f,i}. \tag{3.11}$$

Table 3.2. Thermodynamic data of the reactive species.

	a_1	$a_2(\times 10^3)$	$a_3(\times 10^6)$	$a_4(\times 10^9)$	$a_5(\times 10^{12})$	$b_1(\times 10^{-4})$	b_2
CO	3.58	-0.61	1.02	0.91	-0.90	-1.43	3.51
H_2	2.34	7.98	-19.5	20.2	-7.38	-0.092	0.68
CO_2	2.36	8.98	-7.12	2.46	-0.14	-4.84	9.90
H_2O	4.20	-2.04	6.52	-5.49	1.77	-3.03	-0.85
CH_3OH	5.72	-15.2	65.2	-71.1	26.1	-2.56	-1.50
CH_3OCH_3	5.31	-2.14	53.1	-62.3	23.1	-2.40	7.13

Thermodynamic constants used in Equations (3.8) and (3.9) are presented in Table 3.2, whereas computed reaction equilibrium constants in the operating temperature range is available in Table 3.3.

Table 3.3. Reaction equilibrium constants at different temperatures, $K_{D,rxn}$

rxn	493 K	503 K	513 K	523 K	533 K	543 K
1	5.15×10^{-5}	3.89×10^{-5}	2.97×10^{-5}	2.28×10^{-5}	1.77×10^{-5}	1.38×10^{-5}
2	6.70×10^{-3}	8.13×10^{-3}	9.78×10^{-3}	1.17×10^{-2}	1.39×10^{-2}	1.63×10^{-2}
3	8.10×10^{-3}	5.04×10^{-3}	3.19×10^{-3}	2.05×10^{-3}	1.34×10^{-3}	8.91×10^{-4}
4	24.46	21.99	19.87	18.02	16.41	15.00

Since rate expressions are expressed in terms of component fugacities, Lewis law is adopted to estimate component fugacities as

$$f_i = y_i f_{pure,i}, f_{pure,i} = exp\left[\left(b_i - \frac{a_i}{RT}\right)\frac{p}{RT} ln(p)\right] \tag{3.12}$$

where Table 3.4 provides necessary constants for the pertinent species.

Table 3.4. The van der Waals coefficients of species needed in Equation (3.12).

	$a_i(bar\ L^2\ mol^{-2})$	$b_i(L\ mol^{-1})$
CO	1.472	0.03948
H_2	0.2453	0.02651
CO_2	3.658	0.04286
H_2O	5.537	0.03049
CH_3OH	9.472	0.06584
CH_3OCH_3	5.69	0.07742

Temperature dependence of reaction rate constants and adsorption equilibrium constants are provided in the following tables.

Table 3.5. Temperature dependence of the rate constants ($k_{rxn} = Aexp(B/RT)$) [63].

rxn	A	B	Unit*
1	1.52×10^{-33}	-2.66×10^{5}	mol g_{cat} s^{-1} $bar^{-3/2}$
2	9.04×10^{8}	-1.13×10^{5}	mol g_{cat} s^{-1} bar^{-1}
3	4.06×10^{-6}	-1.17×10^{4}	mol g_{cat} s^{-1} $bar^{-3/2}$
4	1.90×10^{-3}	4.08×10^{3}	mol g_{cat} s^{-1} bar^{-2}

Table 3.6. Adsorption equilibrium constants of the pertinent species [63].

$K_i = Aexp(B/RT)$	A	B	Unit*
K_{CO}	8.40×10^{-11}	1.18×10^{5}	bar^{-1}
K_{CO_2}	1.72×10^{-10}	8.13×10^{4}	bar^{-1}
$K_{H_2O}/K_{H_2}{}^{1/2}$	4.37×10^{-12}	1.15×10^{5}	bar^{-1}
K'_{H_2O}	8.35	3.89×10^{-5}	bar^{-1}
K_{CH_3OH}	9.46	1.13×10^{-3}	bar^{-1}

3.3. Membrane Model

Methodology outlined by Ji *et al.* [67] constitutes the basis of the membrane model whose domain is presented in Figure 3.2. A discontinuity in Navier-Stoke equations is created by a zero-thickness wall between channels to ensure that only user-defined source terms determine the mass transfer across channels. Mesh cells that neighbor zero-thickness wall are designated as source zone for permeate side and sink zone for the reaction channel. Mass transfer across membrane is implemented by defining source terms in these regions which are quantified by a user-defined function and integrated to the existing framework. Fick's Law is used to compute cross-membrane mass flux as

$$J_i = Perm_i(p_{rxn}{}^i - p_{perm}{}^i). \tag{3.13}$$

User-defined function (UDF) involves obtaining partial pressures of the permeable species (i=H_2 or H_2O) for a mesh cell in sink zone ($p_{rxn}{}^i$) and neighboring mesh cell in the sink zone ($p_{perm}{}^i$).

Multiplication of their difference by the membrane permeance yields cross-membrane mass flux in units of mol m^{-2} s^{-1}. Since source terms need to be defined in kg m^{-3} s^{-1}, molecular weight of the species and length of a mesh cell edge are also considered as

$$S_i = \frac{J_i M_i}{l_{\text{edge}}}. \tag{3.14}$$

A user defined memory (UDM) is defined to store the values of the source terms in cell centroid. Instead of calculating source terms for both sides of the zero-thinkness wall, UDM is multiplied by -1 and defined as the source term in the neighboring mesh cell. This approach ensures that the total mass is conserved in the entire solution domain. Since mesh cells in the source zone are identical to those in the permeate channel apart from the source terms, intersection between permeate channel and source zone is defined as the interior boundary condition. The same condition is also applied to the surface between the sink zone and the reaction channel.

Steam permeance and permselectivity ($S_{H_2O/i}$) are the two key properties of the membrane material. Due to very high (3.3×10^3 m^2 m^{-3}) membrane surface area per reactor volume, the former property is of secondary importance for a microchannel reactor. On the other hand, the slippage of reactants or methanol to the permeate channel could diminish the reactor performance significantly [55]. Based on these considerations membrane material is selected as SOD, which offers excellent permselectivities (S_{H_2O/CH_3OH}=233, $S_{H_2O/DME}$=253, S_{H_2O/CO_2}=22.6). At 473 K, H_2O permeance and steam-hydrogen permselectivity (S_{H_2O/H_2}) values are reported as 6.5×10^{-8} mol m^{-2} s^{-1} Pa^{-1} and 4.6, respectively. On the other hand, steam permeance value is assumed as 3.0×10^{-8} mol m^{-2} s^{-1} Pa^{-1} in the simulations based on three considerations. Membrane property data is not available for temperatures higher than 473 K which creates uncertainties for the system. Secondly, multicomponent nature of the reactant flow can lead to surface competitive adsorption and other detrimental factors resulting in poorer membrane performance [67]. Thirdly, since steam content in a mesh cell is limited, mass created in the source zone can be higher than mass disappearing in the sink zone at high permeance values.

As a result, increasing the number of iterations fails to decrease residuals of species conservation equations and continuity equation to an acceptable level.

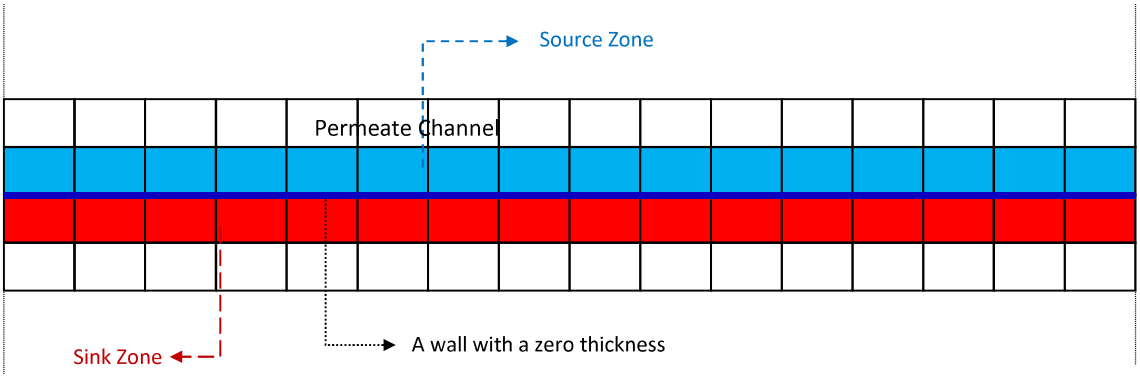

Figure 3.2. Implementation of the membrane model via zone partitioning.

3.4. Solution Methodology and Associated Equations

A two-dimensional (2D) steady state mathematical model involving catalytic reactions, membrane mass transfer, convective and diffusive transport of species and reactive transport within catalyst layer is created to simulate proposed membrane microchannel reactor illustrated in Figure 3.1.

In the case of adiabatic modeling (Section 4.2), convective heat transfer in fluid phases, inter-channel heat exchange through membrane, and heat transfer from catalyst layer are also considered. Relevant conservation equations are presented in Table 3.7. It should be noted that Equations (3.23-3.25) are not considered in the mathematical model unless adiabatic simulations are performed (Section 4.2).

Table 3.7. Reactor model equations (FP: Fluid phases in reaction and permeate channels, CP: Porous catalyst phase in reaction channels; ML: membrane layer between permeate and reaction channels).

Continuity equation	$\nabla.(\vec{v})=0$	(3.18)
Momentum equation (FP)	$\nabla.(\rho_m\vec{v}\vec{v})=\nabla p+\nabla.[\mu_m(\nabla\vec{v}+(\nabla\vec{v})^T)-\frac{2}{3}(\nabla.\vec{v})\mathbf{I}]$	(3.19)
Momentum equation (CP)	$\nabla.(\rho_m\vec{v}\vec{v})=\vec{F}-\nabla p+\nabla.[\mu_m(\nabla\vec{v}+(\nabla\vec{v})^T)-\frac{2}{3}(\nabla.\vec{v})\mathbf{I}]$ $\vec{F}=(\frac{\mu_m}{\alpha}\vec{v}+\frac{C_2}{2}\rho_m\lvert\vec{v}\rvert\vec{v})$; $\alpha=\frac{d_p^2}{150}\frac{{\epsilon_{cat}}^3}{(1-\epsilon_{cat})^2}$; $C_2=\frac{3.5}{d_p}\frac{1-\epsilon_{cat}}{{\epsilon_{cat}}^3}$	(3.20)
Species mass equation (FP)	$\nabla.(\rho_m\vec{v}Y_i)=\nabla.\vec{J}_i$; $\vec{J}_i=-\rho_m D_{i,m}\nabla Y_i$	(3.21)
Species mass equation (CP)	$\nabla.(\rho_m\vec{v}Y_i)=\nabla.\vec{J}_i+M_iR_i$; $\vec{J}_i=-\rho_m D_{eff,i,m}\nabla Y_i$ $R_{CO}=r_2-r_3$; $R_{CO_2}=r_1-r_2$; $R_{H_2}=-3r_1-r_2-2r_3$ $R_{CH_3OH}=r_1+r_3$; $R_{CH_3OCH_3}=r_4$; $R_{H_2O}=r_1+r_2+r_4$	(3.22)
Energy equation for FP	$\nabla.(\rho_m c_{p,m}\vec{v}T)=\nabla.(k_m\nabla T)$	(3.23)
Energy equation for CP	$\nabla.(\rho_m c_{p,m}\vec{v}T)=\nabla.(k_{eff}\nabla T)+\sum(-\Delta H_{rxn}r_{rxn})$	(3.24)
Energy equation ML	$\nabla.(k_w\nabla T)=0$	(3.25)

Gambit software (version 2.3.16) is used to create the solution domain representing the unit cell shown in Figure 3.1. The domain is discretized by square mesh cells, where the resulting mesh contains 6×10^5 nodes, 4.8×10^4 cells in the catalyst layer, 2.28×10^5 cells in reaction channel, 1.2×10^4 cells in source/sink zones, and 2.76×10^5 cells in the permeate channel. Feed temperature, gas composition and velocity are defined as the conditions at the channel inlet. Outermost surfaces are defined as wall boundary condition and transport processes through these regions are nullified. The same boundary condition is applied to the zero-thickness wall, described in 3.2, except thickness of the membrane layer and thermal conductivity data are provided manually which are needed to compute the rate of heat conduction through membrane.

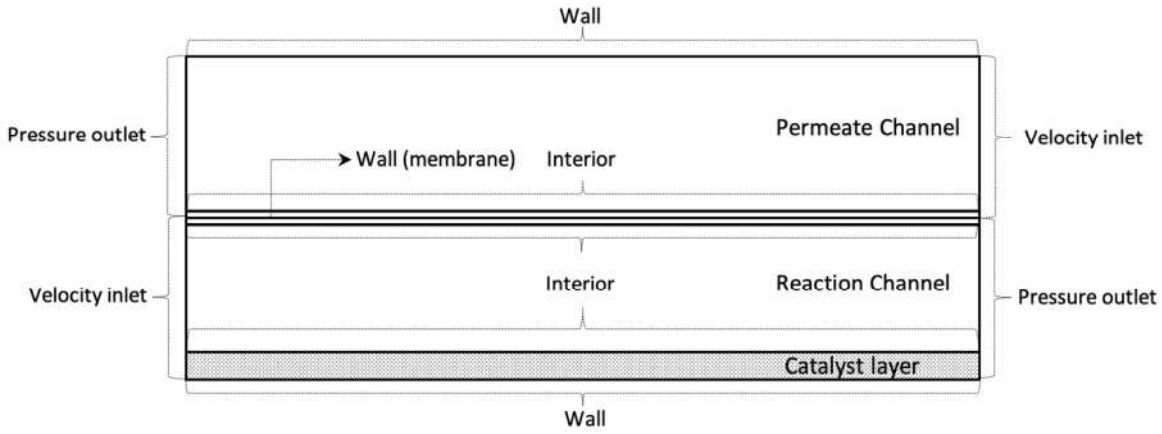

Figure 3.3. Description of the zones and boundary conditions in the solution domain.

Set of property correlations needed to quantify the physical properties of the gas mixture can be found in the literature [12]. These relations, along with the kinetic model (Section 3.2), an the membrane model (Section 3.3) are defined as user-defined functions (UDF) and integrated to the reactor model.

Obtaining flow fields inside the catalyst layer poses some challenges due to very small catalyst particle sizes, since particle-resolved CFD approach requires exact geometry of the porous region. Instead, porous nature of the layer is considered to influence pressure drop, effective thermal conductivity and mass diffusivity within the region. Catalyst layer acts the same way as the other fluid regions apart from the following features:

- Momentum conservation equation includes a momentum source term ($\vec{F}$), formulated in Equation (3.20), to quantify pressure drop caused by the porous nature.
- Effective mass diffusivity of the species are considered to incorporate the effect of Knudsen diffusion within the pores.
- Effect of heat conduction is reflected in energy conservation equations whereas in other fluid regions, this effect is absent.
- Catalytic reactions take place based on the provided UDF.

Temperature, pressure and mixture composition data are processed within each mesh cell to obtain local rate of reactions. Reactive transport within the catalyst layer is modeled based on the quantification of effective mass diffusivity of the reactive species, . Since volumetric reaction rates need to be obtained, catalyst density data is needed. For CZA/HZSM–5=2 the density of the catalyst layer can be calculated as

$$\frac{1}{\rho_{\text{cat}}} = \frac{2/3}{\rho_{\text{CZA}}} + \frac{1/3}{\rho_{\text{HZSM-5}}}. \tag{3.15}$$

Then, density of CZA and HZSM–5 within the catalyst layer can be calculated as

$$\rho_{\text{CZA,mix}} = \frac{2\rho_{\text{cat}}}{3} \tag{3.16}$$

$$\rho_{\text{HZSM-5,mix}} = \frac{1\rho_{\text{cat}}}{3}. \tag{3.17}$$

For default catalyst ratio of CZA/HZSM–5=2, parameters related to catalyst density and physical properties (e.g. porosity, tortuosity) of the porous washcoat layer is presented in Table 3.8.

Table 3.8. Physical properties of the porous catalyst layer

Property	Value	Unit	Reference
k_{cat}	24.2	W m^{-1} K^{-1}	[10]
ϵ_{cat}	0.61	-	[10]
τ_{cat}	1.64	-	[10]
d_{pore}	1.14×10^{-8}	m	[10]
ρ_{CZA}	2.37×10^{3}	kg m^{-3}	[10]
$\rho_{\text{HZSM-5}}$	7.7×10^{2}	kg m^{-3}	[11]
ρ_{cat}	1.34×10^{3}	kg m^{-3}	-
$\rho_{\text{CZA,mix}}$	8.95×10^{2}	kg m^{-3}	-
$\rho_{\text{HZSM-5,mix}}$	4.47×10^{2}	kg m^{-3}	-

4. RESULTS AND DISCUSSION

Effects of key operating parameters such as inlet temperature and pressure, flow direction of the permeate channel, molar inlet CO_2/H_2 ratio, permeate channel inlet velocity and CZA/HZSM-5 mass ratio are studied in the following sections. When a particular parameter is investigated, others are kept at their default values reported in Table 3.1. In addition, validity of the mathematical model and isothermal conditions are tested. Finally, required number of reaction channels and the reactor volume are determined based on a CO_2 to DME pilot plant operated with 1 MW power input. Obtained results provide meaningful insights in designing and operating an actual system.

4.1. Model Verification

Experimental results reported by An *et al.* [63] are used to test the accuracy of the mathematical model. The aforementioned study involves feeding CO_2 and H_2 gas mixture (H_2/CO_2=3) at 483-543 K, 30-50 bar to a reactor containing CZA and HZSM–5 catalysts mixed physically with a mass ratio of 2:1. Space velocity (volumetric flow rate of the inlet gas divided by the catalyst mass) is reported as 6×10^3 ml g_{cat}^{-1} h^{-1}. A parity plot is presented in Figure 4.1, where deviations from the experimental results can be observed.

Both reactor configurations can operate without transport resistances [63,68] which, despite different reactor geometries, allows meaningful comparison. In addition, membrane mass transfer is disabled in the simulations to obtain coherent results. Investigation of Figure 4.1 reveals that the maximum difference between the experimental and predicted CO_2 conversion and DME yield are 5.3% and 8.5%, respectively. Therefore, the mathematical model which is comprised of employed assumptions, thermodynamic relations, property correlations and kinetic model (Equations (3.3), (3.4), (3.5), (3.6)) can be used reliably to predict the behaviour of an actual system.

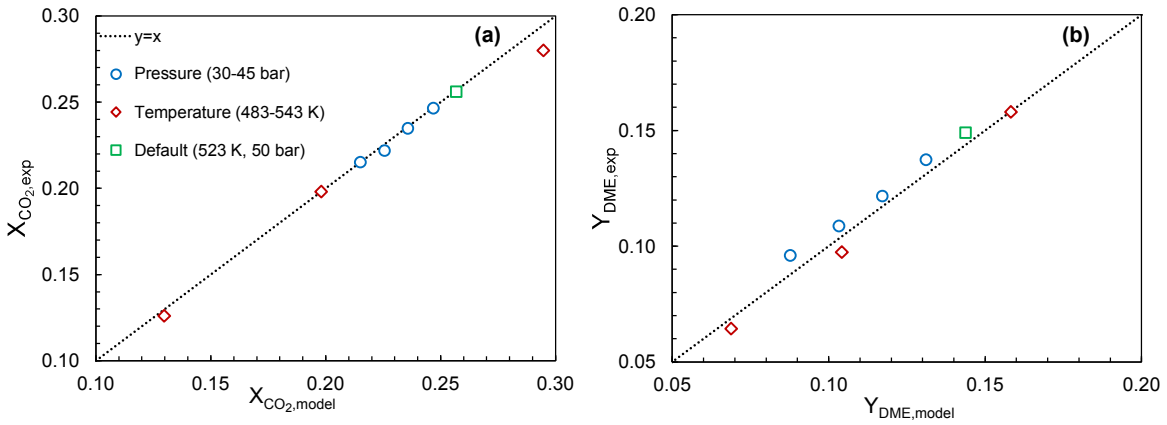

Figure 4.1. Comparison of the experimental and predicted CO_2 conversions and DME yields. Experimental data is taken from [63].

4.2. Validation of the Isothermal Conditions

Heat released by exothermic reactions can be managed effectively using microchannel reactors and near-isothermal conditions are achievable [53, 69]. Therefore, mathematical model assumes that the reactor operates isothermally. To test this assumption, energy conservation equations [68] for fluid and catalyst phases as well as conductive heat transfer through membrane layer are incorporated into the model. Heat fluxes across the outermost boundaries of a unit cell are disabled to ensure adiabatic operation.

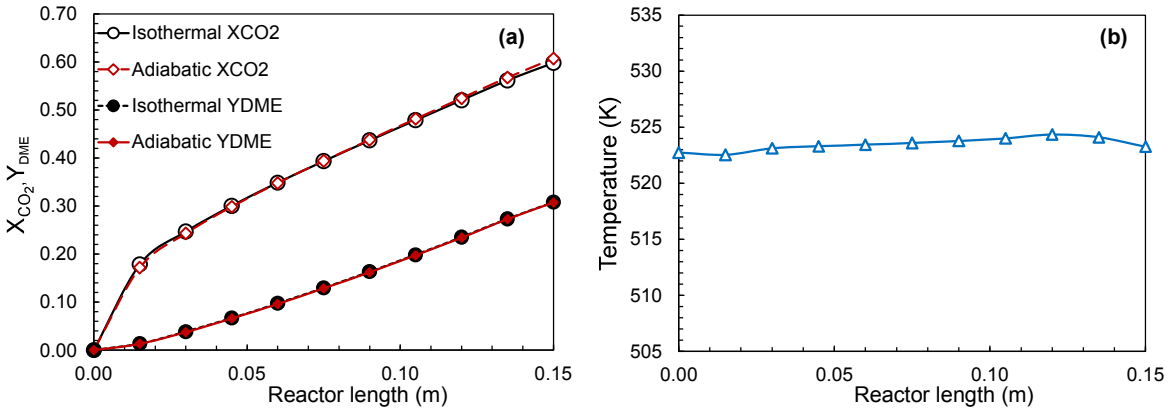

Figure 4.2. Variation of performance metrics under adiabatic and isothermal conditions (a), temperature of the gas mixture along the reactor length (b).

Evolution of CO_2 conversion, DME yield and mixture temperature along the reaction channel are presented in Figure 4.2. Due to negligible (<±1 K) temperature variation in adiabatic case, two configurations have almost identical CO_2 conversion and DME yield. The results point out facile temperature regulation via heat exchange between permeate and reaction channels despite the presence of both endothermic (Reaction (2.2)) and exothermic (Reactions (2.1), (2.3), (2.4)) reactions. Therefore, neglecting computationally expensive energy conservation equations is justified.

4.3. Impact of Inlet Temperature and Pressure

Membrane integrated and membraneless configurations are simulated at 503–543 K and 30–50 bar to investigate the influence of inlet temperature and presssure. Performance metrics are found to improve at increased temperature or pressure for both configurations (Figure 4.3). Since hydrogenation reactions involve products having fewer number of mole species compared to reactants, higher equilibrium conversions can be obtained by increasing the operating pressure. In addition, such a change would increase the reactant partial pressures and boost the rate of reactions. Due to dependence of rate constants on temperature, a similar promotion on reaction kinetics can be achieved by adopting higher inlet temperatures. Reactor performance is maximized at 543 K and 50 bar, resulting CO_2 conversion and DME yield of 73.3% and 34.5%, respectively with membrane integration, and 29.5% and 15.8%, respectively without a membrane. Additionally, incremental change on temperature or pressure produces much more dramatic improvements in the presence of a membrane. In terms CO_2 conversion and DME yield, a relatively flat trajectory is observed without a membrane, especially towards the reactor exit. On the other hand, as evident in increasing trends along the reactor, membrane allows reactor to preserve its perfomance due to relaxed thermodynamic limitations. Additionally, considering relatively high reactor performance at milder operating conditions, membrane integration offers a robust option to decrease energy consumption in overall process.

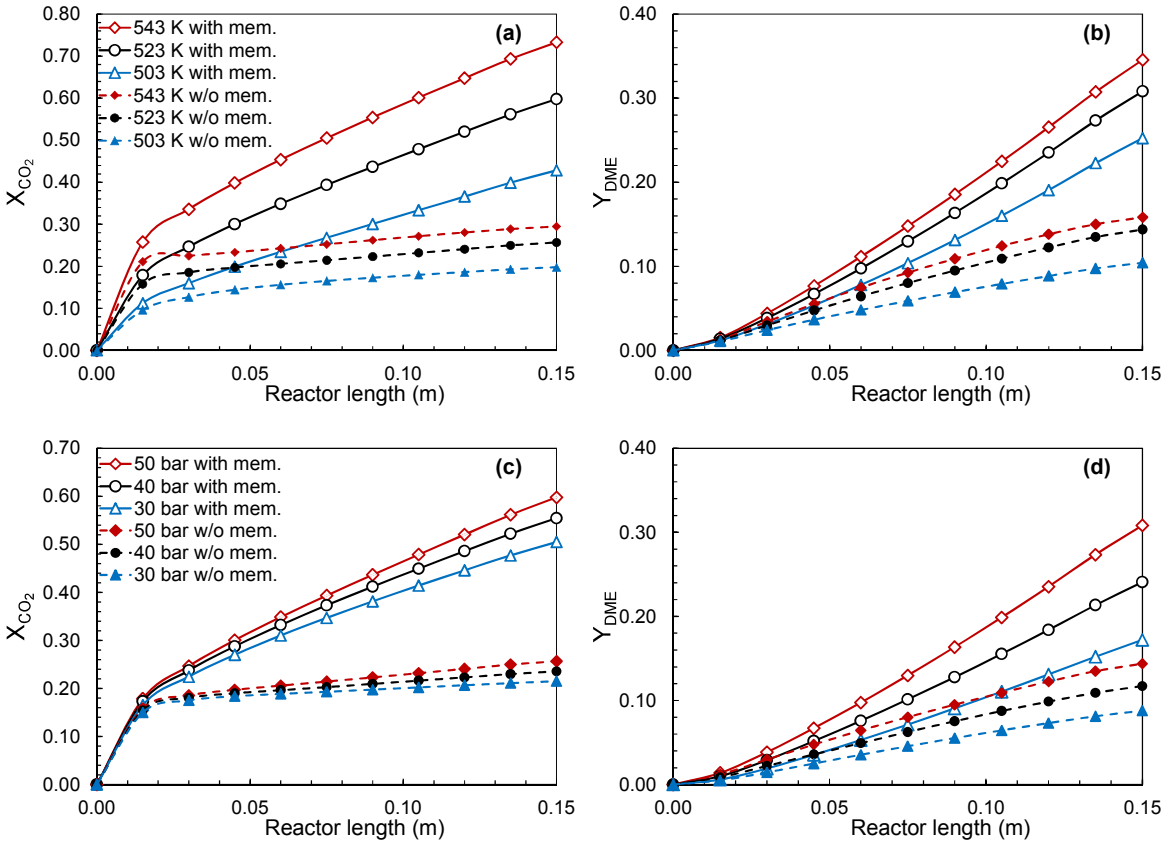

Figure 4.3. Influence of temperature/pressure on CO_2 conversion, DME yield with and without membrane integration.

4.4. Impact of Flow Direction of the Permeate Channel

Evolution of concentration gradient between channels along the reactor can be manipulated by adopting either co-current or counter-current permeate flow. Comparison presented in Figure 4.4 reveals that, unlike nearly identical H_2 flow rate profiles, the behavior of H_2O flow rate is strikingly different for these configurations. Steam content is higher for counter-current flow within the first ~7.5x10^{-2} m of the reaction channel. However, since H_2O continues to build-up in co-current configuration, H_2O flow rate is significantly higher at the outlet of the reaction channel. As a result, average H_2O flow rate is 1.5×10^{-8} mol s^{-1}, which is higher than 8.5×10^{-9} mol s^{-1} obtained when sweep gas fed counter-currently. The dissimilar H_2O flow rate profiles lead to similar divergence in CO_2 conversion and DME yield trends. Even though these metrics are superior for co-current flow in the first 1×10^{-1} m, counter-current configuration leads to better results at the channel exit.

H_2O and H_2 flow rate profiles are also provided for membraneless case in Figure 4.4. In the absence of membrane, H_2 flow rate in a reaction channel decreases due to Reactions (2.1-2.3), conversely, H_2 permeated through membrane causes net increase in H_2 content. Furthermore, SOD membrane is capable to decrease H_2O flow rate by a factor of ~7 towards reactor exit. The beneficial effect of avoiding thermodynamic supression due to steam build-up can be observed just after ~2×10–2 m from the inlet. Up to three times higher CO_2 conversion and DME yield can be obtained with the combined impact of cross–membrane H_2O and H_2 transfer.

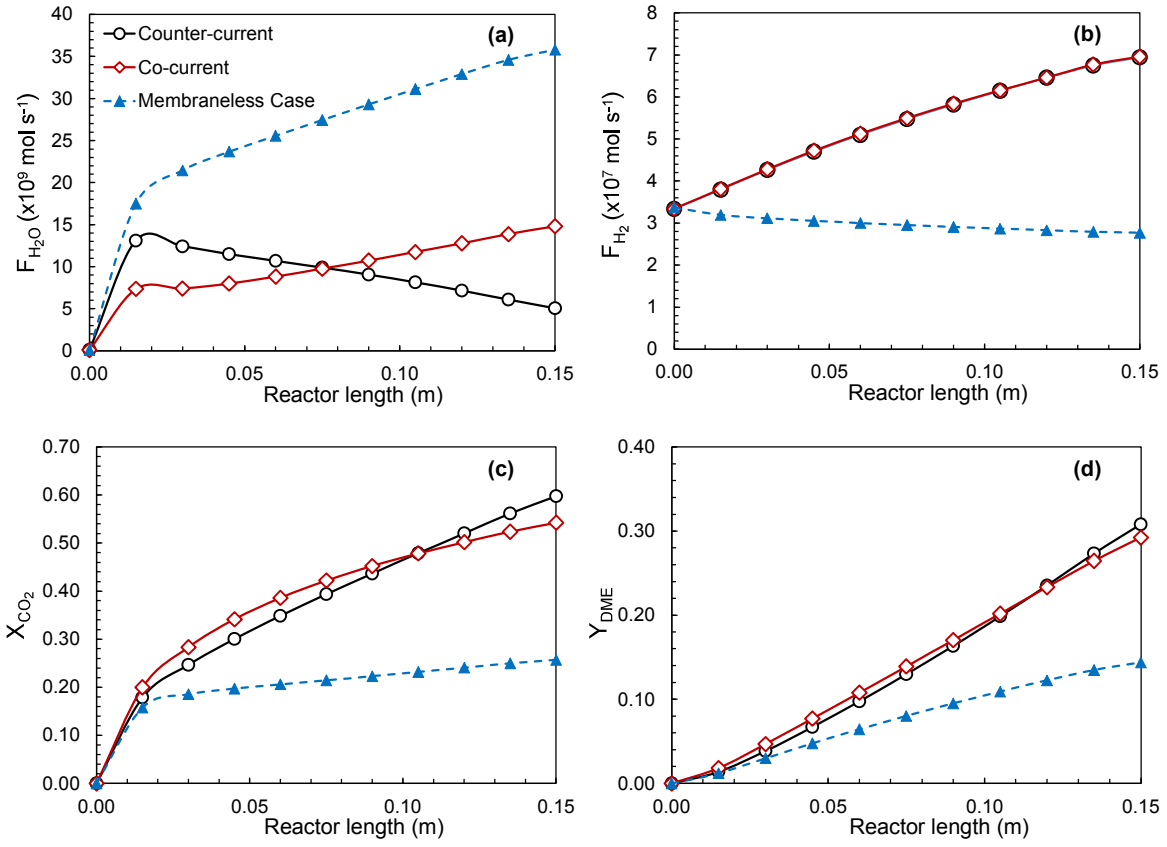

Figure 4.4. Comparison of co-current, counter-current and membraneless configurations in terms of performance metrics and flow rates of H_2O and H_2 along the reactor.

4.5. Impact of H_2/CO_2 Feed Ratio

Considering the strong dependence of hydrogenation kinetics on H_2 partial pressure (Equations (3.3), (3.4), (3.5)), the effect of relative hydrogen content in the reaction channel is investigated by varying molar inlet ratio of H_2/CO_2 within 1-4. When adopting higher H_2/CO_2 ratios, inlet flow rate of CO_2 is decreased to accommodate additional H_2 to keep space velocity constant at 6×10^3 ml g_{cat} s^{-1} and vice versa. Examination of Figure 4.5 reveals that higher H_2/CO_2 ratios lead to superior CO_2 conversion and DME yield. On the other hand, the difference is less remarkable within H_2/CO_2=3-4. Diminishing CO_2 content/partial pressure at higher H_2/CO_2, seems to suppress the rate of Reaction (2.2) despite higher H_2 concentration. Such a variation in inlet CO_2 flow rates is also responsible for the dependence of total amount of CO_2 consumed and DME produced in a reaction channel on H_2/CO_2 ratio. 1.4, 1.7 and 1.8×10^{-8} mol s^{-1} DME is synthesized and 8.9, 6.7 and 6.1×10^{-8} mol s^{-1} CO_2 is consumed at H_2/CO_2 of 1, 3 and 4, respectively. Considering the trade-off between the amount of CO_2 consumed and DME produced, optimal H_2/CO_2 ratio should be determined based on a detailed techno-economic analysis.

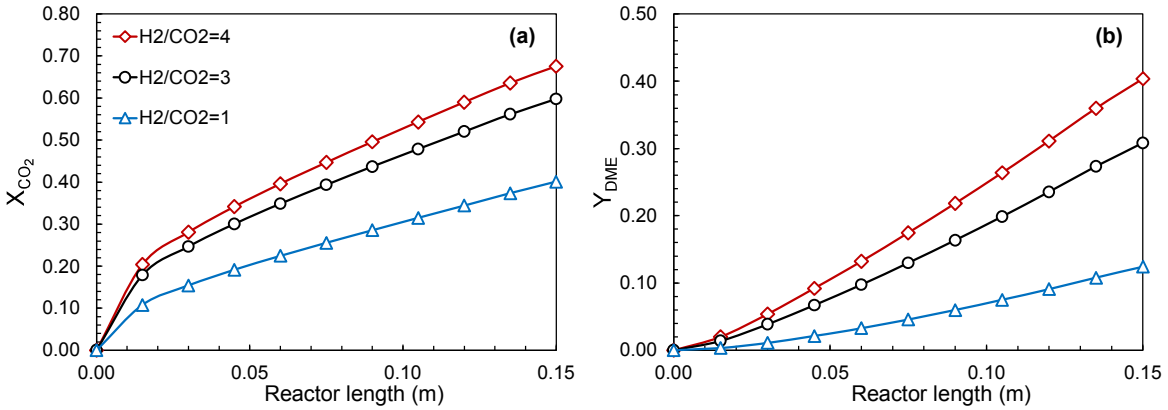

Figure 4.5. Influence of molar inlet H_2/CO_2 ratio on reactor performance.

4.6. Effect of the inlet velocity of the permeate stream

Magnitudes of inlet velocities of reaction and permeate channels at default operation are given in Table 3.1.

The ratio of these values, defined as (v_{rat}), is varied between 5 and 20 to study the impact of sweep H_2 flow rate. At low sweep H_2 flow, membrane performance suffers since concentration of H_2O on the permeate side would approach to the values observed in the reaction channel. At the opposite extreme, concentration of H_2O in the sweep mixture would be negligible when very large quantites of H_2 is sent to the permeate channel. In such a configuration, the influx of H_2 towards the reactive mixture is also maximized due to conserved H_2 concentration gradient between channels. As shown in Figure 4.6, increasing v_{rat} from 5 to 10, results in a remarkable improvement on cross-membrane mass transport. Consequently, both DME yield and CO_2 conversion increases. On the other hand, considering the diminished improvement and the cost associated with conditioning and dosing additional H_2, increasing v_{rat} beyond 10 seems impractical.

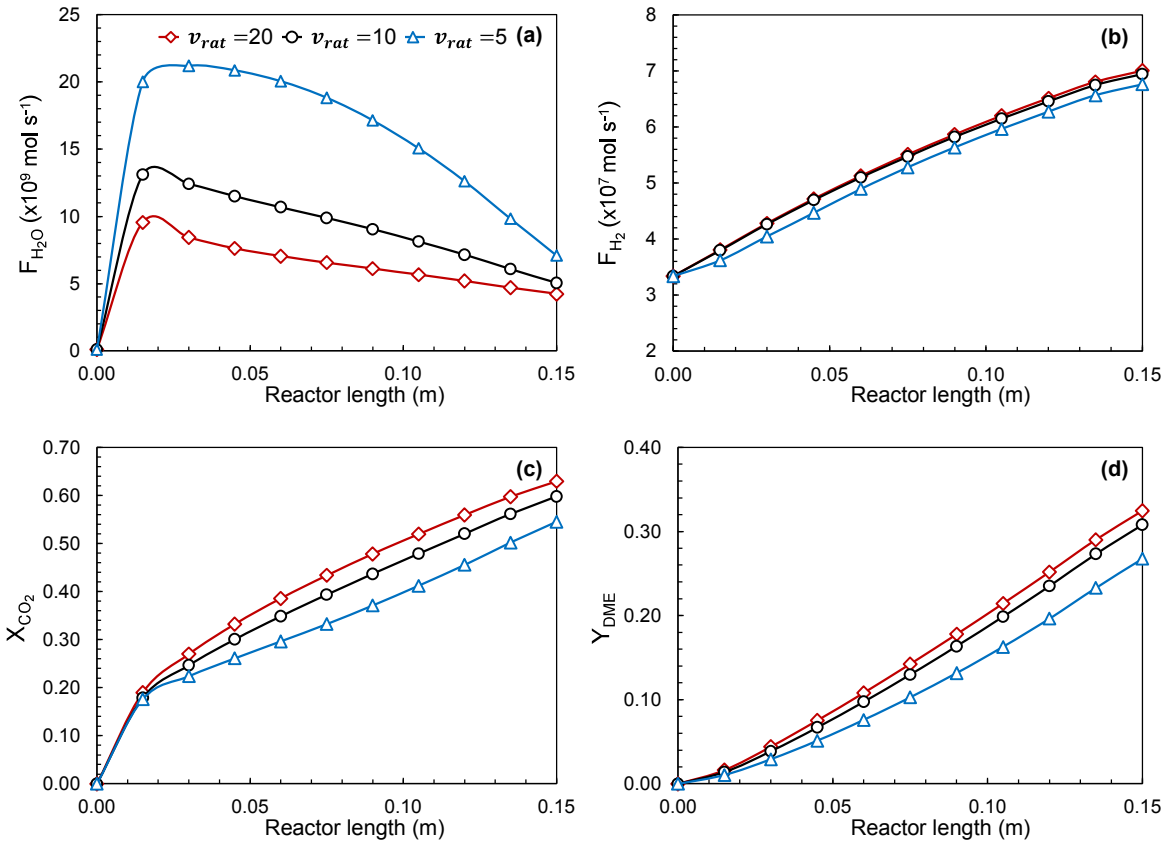

Figure 4.6. Evolution of CO_2 conversion, DME yield and flow rates permeable species along the reactor at different v_{rat} values.

One can speculate that, rather than setting v_{rat}=10, a better reactor performance can be achieved by sending a portion of sweep H_2 to the reaction channel. Such a configuration would lead to higher H_2/CO_2 ratios whose benefits are reported in Section 4.5. To test this hypothesis, a new variable called H_2 flow ratio, which is defined as the flow rate of H_2 diverted to the reaction channel divided by the amount of H_2 sent to permeate channel at default operation. In other words, H_2 flow ratio of 0.9 implies that 10% of the original sweep H_2 is fed to the reaction channel and the remaining 90% is kept at permeate side.

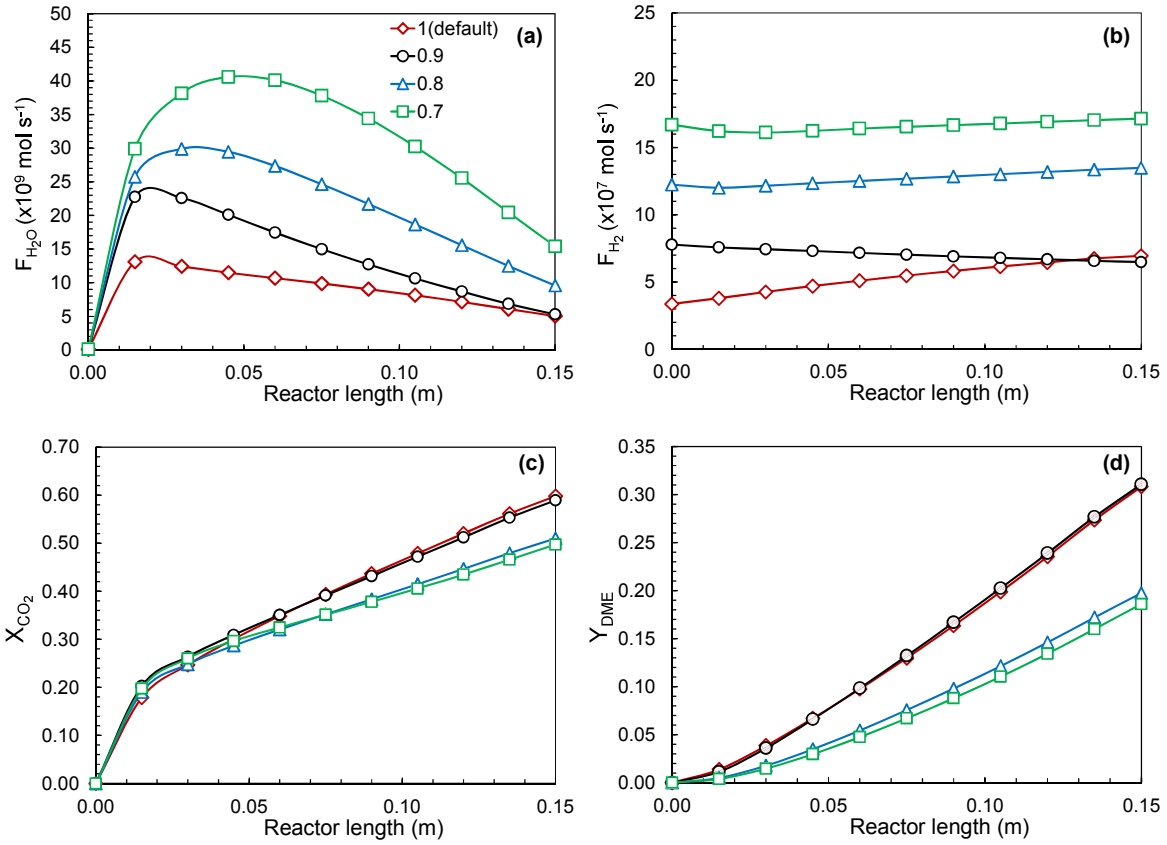

Figure 4.7. Effect of hydrogen flow ratio on performance metrics and flow rates of H_2O and H_2 along the reactor.

Flow ratio is varied between 0.7 and 1 and the results are presented in Figure 4.7. When flow ratio is set to 0.7, H_2 flow rate in the reactive mixture increases substantially and up to $H_2/CO_2 \approx 30$ can be reached towards the reactor exit.

However, this configuration leads to significant accumulation of H_2O due to unsatisfactory membrane performance linked to low v_{rat}. Similar reactor performances observed at flow ratios of 0.9 and 1, indicates a perfect balance between the competing effects of H_2/CO_2 ratio and v_{rat}.

4.7. Impact of Catalyst Ratio

Considering the dimensions of a reaction channel (Section 3.1), a single washcoated catalyst layer has a volume of 4.5×10^{-9} m^3 which can accommodate catalyst mixtures with various compositions. Relative rate of methanol formation and its dehydration can be manipulated by varying the relative amounts of Cu-ZnO-Al_2O_3 and HZSM-5 in the catalyst mixture. Densities of Cu-ZnO-Al_2O_3 and HZSM-5 are 2.4×10^3 and 7.7×10^2 kg $^{-1}$ m respectively, which implies total mass of catalyst would be higher as CZA/HZSM-5 is increased. Therefore, inlet flow rate of reactants are adjusted to keep space velocity constant at 6×10^3 ml g_{cat}^{-1} h^{-1}. Changing catalyst ratio from CZA/HZSM-5=1 to 3 increases converted CO_2 amount from 5.0 to 7.7×10^{-8} mol s^{-1} even though the improvement in fractional CO_2 conversion remain insignificant (Figure 4.8). On the other hand, since rate of methanol dehydration depends on both partial pressure of methanol and the amount of dehydration catalyst, changing CZA/HZSM-5 creates two competing effects on DME yield. Since highest DME yield is obtained at CZA/HZSM-5=3 it can be deduced that, higher methanol partial pressures fueled by increased CZA content dominates the negative influence of diminished amount of dehydration catalyst. Considering these findings, it can be concluded that both reactor capacity and performance metrics can be optimized by choosing ideal catalyst composition.

4.8. Sizing of Intensified CO_2 to DME Reactor System

Renewable energy can be utilized to produce so-called green hydrogen via water electrolysis, which is one of the key ingredients of a CO_2 to DME pilot plant [70]. Around 18 kg H_2/h ($\approx$2.5 mol H_2 s^{-1}) can be synthesized with a 1 MW power input which is the power capacity adopted by many pilot projects.

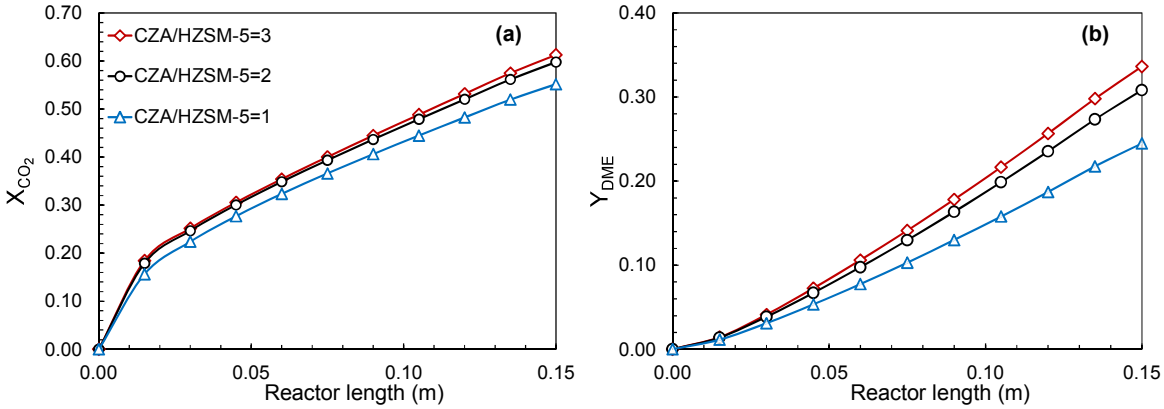

Figure 4.8. Effect of catalyst mass ratio on CO_2 conversion and DME yield.

The number of required unit cells can be estimated based on the H_2 consumption of a single cell assuming no H_2 is lost during separation and recycle stages. Based on this approach, 1.1×10^{7} reaction channels are needed. Assuming the thickness of the membrane layer and the horizontal distance between adjacent channels are 1×10^{-3} m, target capacity can be reached with eight compact reactor blocks (W&H≈2.4 m, L=1.5×10^{-1} m) with a total volume of 6.9 m^{-3}. Around 1×10^{3} tons of CO_2 can be converted into 2.76×10^{2} tons of DME, 35 tons of methanol and 2.8 $\times10^{2}$ tons of CO annually based on such sizing. It should be noted that the present study focuses only on the reactor unit, and potential CO_2 emissions due to energy requirement of feed conditioning and product separation should be considered in a separate study.

5. CONCLUSION

5.1. Conclusions

Direct DME synthesis via CO_2 hydrogenation is investigated in a membrane microchannel reactor. A repeating unit cell contains a steam selective SOD membrane layer which is sandwiched between a reaction channel and a parallel permeate channel. The inner walls of a reaction channel are washcoated with a physical mixture Cu-ZnO-Al_2O_3 and HZSM-5 catalysts with a 3:1 mass ratio, where the former is responsible for methanol synthesis and the latter dehydrates methanol to DME. In default operation, H_2-CO_2 gas mixture (H_2/CO_2=3) is fed to the reaction channel with a space velocity of 6×10^3 ml $gcat^{-1}$ h^{-1} and pure H_2 is dosed to the permeate channel to sweep permeated H_2O. An isothermal steady state reactor model which considers two dimensional conservation of momentum, species mass transport, membrane mass transfer and reactive transport within the porous catalyst layer is solved using finite volume method under ANSYS platform. Validation of isothermal conditons is performed by incorporating energy conservation equations to the reactor model which resulted in near-constant temperature profile. The following are the other key conclusions obtained from this work:

- Reactor performance can be improved by increasing temperature or pressure. Membrane integration enhances CO_2 conversion and DME yield by a factor of > 3. Furthermore, reactor responds to changes in temperature and pressure more strongly when the membrane layer is present.
- Higher inlet H_2/CO_2 ratios promote CO_2 conversion and DME yield. However, the highest amount of CO_2 is converted when H_2/CO_2=1.
- Membrane mass transfer and reactor performance depends strongly on the flow rate of the permeate channel which is quantified by the relative inlet velocity magnitude (v_{rat}). However, the benefits becomes insignificant for $v_{rat}>10$. Dosing a portion of sweep H_2 to the reaction channel does not lead to a better reactor performance due to diminished H_2O removal capability dominating the positive impact of higher H_2/CO_2 ratio.

- Counter-current flow configuration offers slightly superior H_2O removal capability compared to co-current flow which affects reactor performance in a positive way.
- Both reactor capacity and performance metrics (CO_2 conversion and DME yield) can be altered by varying the CZA/HZSM–5 mass ratio. Reactor performance is maximized at CZA/HZSM–5=3.
- Eight microchannel reactor blocks having total a volume of 6.9 m^{-3} are capable of converting 1×10^3 tons of CO2 a year into 2.76×10^2 tons of DME using H_2 input from 1 MW electrolyzer.

5.2. Recommendations

- Other methanol synthesis and/or dehydration catalysts can be modeled and the results can be compared with the CZA-HZSM-5 mixture.
- The impacts of membrane permeance and permselectivities can be investigated using different membrane materials.
- Volumetric miniaturization can be studied by varying the channel dimensions.
- A membrane model based on Maxwell-Stefan diffusion can be created to obtain a more realistic membrane simulation.
- The impact of catalyst deactivation can be studied by adopting an unsteady state reactor model and compatible kinetic expressions.

REFERENCES

1. Ellabban, O., H. Abu-Rub and F. Blaabjerg, "Renewable Energy Resources: Current Status, Future Prospects and Their Enabling Technology", *Renewable and Sustainable Energy Reviews*, Vol. 39, pp. 748–764, 2014.

2. Baena-Moreno, F. M., M. Rodríguez-Galán, F. Vega, B. Alonso-Fariñas, L. F. Vilches Arenas and B. Navarrete, "Carbon Capture and Utilization Technologies: a Literature Review and Recent Advances", *Energy Sources, Part A: Recovery, Utilization, and Environmental Effects*, Vol. 41, No. 12, pp. 1403–1433, 2019.

3. Arcoumanis, C., C. Bae, R. Crookes and E. Kinoshita, "The Potential of Di-methyl Ether (DME) as an Alternative Fuel for Compression-ignition Engines: A Review", *Fuel*, Vol. 87, No. 7, pp. 1014–1030, 2008.

4. Ge, Q., Y. Huang, F. Qiu and S. Li, "Bifunctional Catalysts for Conversion of Synthesis Gas to Dimethyl Ether", *Applied Catalysis A: General*, Vol. 167, No. 1, pp. 23–30, 1998.

5. Azizi, Z., M. Rezaeimanesh, T. Tohidian and M. R. Rahimpour, "Dimethyl Ether: A Review of Technologies and Production Challenges", *Chemical Engineering and Processing: Process Intensification*, Vol. 82, pp. 150–172, 2014.

6. Venvik, H. J. and J. Yang, "Catalysis in Microstructured Reactors: Short Review on Small-scale Syngas Production and Further Conversion into Methanol, DME and Fischer-Tropsch Products", *Catalysis Today*, Vol. 285, pp. 135–146, 2017.

7. Göransson, K., U. Söderlind, J. He and W. Zhang, "Review of Syngas Production via Biomass DFBGs", *Renewable and Sustainable Energy Reviews*, Vol. 15, No. 1, pp. 482–492, 2011.

8. Iliuta, I., F. Larachi and P. Fongarland, "Dimethyl Ether Synthesis with in situ H2O Removal in Fixed-bed Membrane reactor: Model and Simulations", *Industrial & Engi-*

neering Chemistry Research, Vol. 49, No. 15, pp. 6870–6877, 2010.

9. van Kampen, J., J. Boon, F. van Berkel, J. Vente and M. van Sint Annaland, "Steam Separation Enhanced Reactions: Review and Outlook", *Chemical Engineering Journal*, Vol. 374, pp. 1286–1303, 2019.

10. Mardanpour, M. M., R. Sadeghi, M. R. Ehsani and M. N. Esfahany, "Enhancement of Dimethyl Ether Production with Application of Hydrogen-permselective Pd-based Membrane in Fluidized Bed Reactor", *Journal of Industrial and Engineering Chemistry*, Vol. 18, No. 3, pp. 1157–1165, 2012.

11. Koybasi, H. H. and A. K. Avci, "Modeling of a Membrane Integrated Catalytic Microreactor for Efficient DME Production from Syngas with CO2", *Catalysis Today*, Vol. 383, pp. 133–145, 2022.

12. Koybasi, H. H., C. Hatipoglu and A. K. Avci, "Sustainable DME Synthesis from CO2–rich Syngas in a Membrane Assisted Reactor–Microchannel Heat Exchanger System", *Journal of CO2 Utilization*, Vol. 52, p. 101660, 2021.

13. Saravanan, K., H. Ham, N. Tsubaki and J. W. Bae, "Recent Progress for Direct Synthesis of Dimethyl Ether from Syngas on the Heterogeneous Bifunctional Hybrid Catalysts", *Applied Catalysis B: Environmental*, Vol. 217, pp. 494–522, 2017.

14. Chen, W.-H., C.-L. Hsu and X.-D. Wang, "Thermodynamic Approach and Comparison of Two-step and Single Step DME (Dimethyl Ether) Syntheses with Carbon Dioxide Utilization", *Energy*, Vol. 109, pp. 326–340, 2016.

15. Hosseininejad, S., A. Afacan and R. Hayes, "Catalytic and Kinetic Study of Methanol Dehydration to Dimethyl Ether", *Chemical Engineering Research and Design*, Vol. 90, No. 6, pp. 825–833, 2012.

16. Volkov, V., E. Novitskii, G. Dibrov, P. Samokhin, M. Kipnis and A. Yaroslavtsev, "Catalytic Conversion of Methanol to Dimethyl Ether on Polymer/ceramic Composite Mem-

branes", *Catalysis Today*, Vol. 193, No. 1, pp. 31–36, 2012.

17. Liu, Y., S. Podila, D. L. Nguyen, D. Edouard, P. Nguyen, C. Pham, M. J. Ledoux and C. Pham-Huu, "Methanol Dehydration to Dimethyl Ether in a Platelet Milli-reactor Filled with H-ZSM5/SiC Foam Catalyst", *Applied Catalysis A: General*, Vol. 409, pp. 113–121, 2011.

18. Mao, D., W. Yang, J. Xia, B. Zhang and G. Lu, "The Direct Synthesis of Dimethyl Ether from Syngas over Hybrid Catalysts with Sulfate-modified γ-alumina as Methanol Dehydration Components", *Journal of Molecular Catalysis A: Chemical*, Vol. 250, No. 1-2, pp. 138–144, 2006.

19. Raoof, F., M. Taghizadeh, A. Eliassi and F. Yaripour, "Effects of Temperature and Feed Composition on Catalytic Dehydration of Methanol to Dimethyl Ether over γ-alumina", *Fuel*, Vol. 87, No. 13-14, pp. 2967–2971, 2008.

20. Yaripour, F., F. Baghaei, I. Schmidt and J. Perregaard, "Catalytic Dehydration of Methanol to Dimethyl Ether (DME) over Solid-acid Catalysts", *Catalysis Communications*, Vol. 6, No. 2, pp. 147–152, 2005.

21. Xu, M., J. H. Lunsford, D. W. Goodman and A. Bhattacharyya, "Synthesis of Dimethyl Ether (DME) from Methanol over Solid-acid Catalysts", *Applied Catalysis A: General*, Vol. 149, No. 2, pp. 289–301, 1997.

22. Ramos, F., A. D. De Farias, L. E. P. Borges, J. Monteiro, M. A. Fraga, E. F. Sousa-Aguiar and L. G. Appel, "Role of Dehydration Catalyst Acid Properties on One-step DME Synthesis over Physical Mixtures", *Catalysis Today*, Vol. 101, No. 1, pp. 39–44, 2005.

23. Fei, J., Z. Hou, B. Zhu, H. Lou and X. Zheng, "Synthesis of Dimethyl Ether (DME) on Modified HY Zeolite and Modified HY Zeolite-supported Cu–Mn–Zn Catalysts", *Applied Catalysis A: General*, Vol. 304, pp. 49–54, 2006.

24. Moradi, G., F. Yaripour and P. Vale-Sheyda, "Catalytic Dehydration of Methanol to Dimethyl Ether over Mordenite Catalysts", *Fuel Processing Technology*, Vol. 91, No. 5, pp. 461–468, 2010.

25. Tokay, K. C., T. Dogu and G. Dogu, "Dimethyl Ether Synthesis over Alumina Based Catalysts", *Chemical Engineering Journal*, Vol. 184, pp. 278–285, 2012.

26. Gates, B. and L. Johanson, "Langmuir-Hinshelwood Kinetics of the Dehydration of Methanol Catalyzed by Cation Exchange Resin", *AIChE Journal*, Vol. 17, No. 4, pp. 981–983, 1971.

27. Kiviranta-Pääkkönen, P. K., L. K. Struckmann, J. A. Linnekoski and A. O. I. Krause, "Dehydration of the Alcohol in the Etherification of Isoamylenes with Methanol and Ethanol", *Industrial & Rngineering Chemistry Research*, Vol. 37, No. 1, pp. 18–24, 1998.

28. Zhang, L., W. Junhua, W. Pei, H. Zhaoyin, F. Jinhua and X. Zheng, "Synthesis of Dimethyl Ether via Methanol Dehydration over Combined Al2O3-HZSM-5 Solid Acids", *Chinese Journal of Catalysis*, Vol. 31, No. 8, pp. 987–992, 2010.

29. Zhu, Y., S. Wang, X. Ge, Q. Liu, Z. Luo and K. Cen, "Experimental Study of Improved Two Step Synthesis for DME Production", *Fuel Processing Technology*, Vol. 91, No. 4, pp. 424–429, 2010.

30. Aguayo, A. T., J. , D. Mier, J. M. Arandes, M. Olazar and J. Bilbao, "Kinetic Modeling of Dimethyl Ether Synthesis in a Single step on a CuO- ZnO- Al2O3/γ-Al2O3 Catalyst", *Industrial & Engineering Chemistry Research*, Vol. 46, No. 17, pp. 5522–5530, 2007.

31. Ereña, J., I. Sierra, M. Olazar, A. G. Gayubo and A. T. Aguayo, "Deactivation of a CuO- ZnO- Al2O3/γ-Al2O3 Catalyst in the Synthesis of Dimethyl Ether", *Industrial & Engineering Chemistry Research*, Vol. 47, No. 7, pp. 2238–2247, 2008.

32. Kang, S.-H., J. W. Bae, H.-S. Kim, G. M. Dhar and K.-W. Jun, "Enhanced Catalytic

Performance for Dimethyl Ether Synthesis from Syngas with the Addition of Zr or Ga on a Cu- ZnO- Al2O3/γ-Al2O3 Bifunctional Catalyst", *Energy & Fuels*, Vol. 24, No. 2, pp. 804–810, 2010.

33. Wang, Y., W. Wang, Y. Chen, J. Ma and R. Li, "Synthesis of Dimethyl Ether from Syngas over Core–shell Structure Catalyst CuO–ZnO–Al2O3@ SiO2–Al2O3", *Chemical Engineering Journal*, Vol. 250, pp. 248–256, 2014.

34. Phienluphon, R., K. Pinkaew, G. Yang, J. Li, Q. Wei, Y. Yoneyama, T. Vitidsant and N. Tsubaki, "Designing Core (Cu/ZnO/Al2O3)–shell (SAPO-11) Zeolite Capsule Catalyst with a Facile Physical Way for Dimethyl Ether Direct Synthesis from Syngas", *Chemical Engineering Journal*, Vol. 270, pp. 605–611, 2015.

35. Lee, Y. J., M. H. Jung, J.-B. Lee, K.-E. Jeong, H.-S. Roh, Y.-W. Suh and J. W. Bae, "Single-step Synthesis of Dimethyl Ether from Syngas on Al2O3-modified CuO–ZnO–Al2O3/ferrierite Catalysts: Effects of Al2O3 Content", *Catalysis Today*, Vol. 228, pp. 175–182, 2014.

36. Montesano, R., A. Narvaez and D. Chadwick, "Shape-selectivity Effects in Syngas-to-dimethyl Ether Conversion over Cu/ZnO/Al2O3 and Zeolite Mixtures: Carbon Deposition and By-product Formation", *Applied Catalysis A: General*, Vol. 482, pp. 69–77, 2014.

37. Cai, M., V. Subramanian, V. Sushkevich, V. Ordomsky and A. Khodakov, "Effect of Sn Additives on the CuZnAl–HZSM-5 Hybrid Catalysts for the Direct DME Synthesis from Syngas", *Applied Catalysis A: General*, Vol. 502, pp. 370–379, 2015.

38. Ereña, J., I. Sierra, A. T. Aguayo, A. Ateka, M. and J. Bilbao, "Kinetic Modelling of Dimethyl Ether Synthesis from (H2+ CO2) by Considering Catalyst Deactivation", *Chemical Engineering Journal*, Vol. 174, No. 2-3, pp. 660–667, 2011.

39. Naik, S. P., T. Ryu, V. Bui, J. D. Miller, N. B. Drinnan and W. Zmierczak, "Synthesis of

DME from CO2/H2 Gas Mixture", *Chemical Engineering Journal*, Vol. 167, No. 1, pp. 362–368, 2011.

40. Zhang, Y., D. Li, S. Zhang, K. Wang and J. Wu, "CO2 Hydrogenation to Dimethyl Ether over CuO–ZnO–Al2O3/HZSM-5 Prepared by Combustion Route", *RSC Advances*, Vol. 4, No. 32, pp. 16391–16396, 2014.

41. Zhao, Y., J. Chen and J. Zhang, "Effects of ZrO2 on the Performance of CuO-ZnO-Al2O3/HZSM-5 Catalyst for Dimethyl Ether Synthesis from CO2 Hydrogenation", *Journal of Natural Gas Chemistry*, Vol. 16, No. 4, pp. 389–392, 2007.

42. Sun, J. T., I. S. Metcalfe and M. Sahibzada, "Deactivation of Cu/ZnO/Al2O3 Methanol Synthesis Catalyst by Sintering", *Industrial & Engineering Chemistry Research*, Vol. 38, No. 10, pp. 3868–3872, 1999.

43. Hu, J., Y. Wang, C. Cao, D. C. Elliott, D. J. Stevens and J. F. White, "Conversion of Biomass Syngas to DME Using a Microchannel Reactor", *Industrial & Engineering Chemistry Research*, Vol. 44, No. 6, pp. 1722–1727, 2005.

44. Hayer, F., H. Bakhtiary-Davijany, R. Myrstad, A. Holmen, P. Pfeifer and H. J. Venvik, "Modeling and Simulation of an Integrated Micro Packed Bed Reactor-heat Exchanger Configuration for Direct Dimethyl Ether Synthesis", *Topics in Catalysis*, Vol. 54, No. 13-15, p. 817, 2011.

45. Hayer, F., H. Bakhtiary-Davijany, R. Myrstad, A. Holmen, P. Pfeifer and H. J. Venvik, "Synthesis of Dimethyl Ether from Syngas in a Microchannel Reactor—Simulation and Experimental Study", *Chemical Engineering Journal*, Vol. 167, No. 2-3, pp. 610–615, 2011.

46. Hayer, F., H. Bakhtiary-Davijany, R. Myrstad, A. Holmen, P. Pfeifer and H. J. Venvik, "Characteristics of Integrated Micro Packed Bed Reactor-heat Exchanger Configurations in the Direct Synthesis of Dimethyl Ether", *Chemical Engineering and Processing: Pro-*

cess Intensification, Vol. 70, pp. 77–85, 2013.

47. Simsek, E., A. K. Avci and Z. I. Önsan, "Investigation of Catalyst Performance and Microstructured Reactor Configuration for Syngas Production by Methane Steam Reforming", *Catalysis Today*, Vol. 178, No. 1, pp. 157–163, 2011.

48. Simsek, E., M. Karakaya, A. K. Avci and Z. I. Onsan, "Oxidative Steam Reforming of Methane to Synthesis Gas in Microchannel Reactors", *International Journal of Hydrogen Energy*, Vol. 38, No. 2, pp. 870–878, 2013.

49. Kolb, G. and V. Hessel, "Micro-structured Reactors for Gas Phase Reactions", *Chemical Engineering Journal*, Vol. 98, No. 1-2, pp. 1–38, 2004.

50. Kiwi-Minsker, L. and A. Renken, "Microstructured Reactors for Catalytic Reactions", *Catalysis Today*, Vol. 110, No. 1-2, pp. 2–14, 2005.

51. Delparish, A. and A. K. Avci, "Intensified Catalytic Reactors for Fischer-Tropsch Synthesis and for Reforming of Renewable Fuels to Hydrogen and Synthesis Gas", *Fuel Processing Technology*, Vol. 151, pp. 72–100, 2016.

52. Önsan, Z. I. and A. K. Avci, *Multiphase Catalytic Reactors: Theory, Design, Manufacturing, and Applications*, John Wiley & Sons, 2016.

53. Rebrov, E., M. De Croon and J. Schouten, "Design of a Microstructured Reactor with Integrated Heat-exchanger for Optimum Performance of a Highly Exothermic Reaction", *Catalysis Today*, Vol. 69, No. 1-4, pp. 183–192, 2001.

54. Rebrov, E., M. De Croon and J. Schouten, "Development of the Kinetic Model of Platinum Catalyzed Ammonia Oxidation in a Microreactor", *Chemical Engineering Journal*, Vol. 90, No. 1-2, pp. 61–76, 2002.

55. Diban, N., A. M. Urtiaga, I. Ortiz, J. Ereña, J. Bilbao and A. T. Aguayo, "Influence of the Membrane Properties on the Catalytic Production of Dimethyl Ether with in situ Water

Removal for the Successful Capture of CO2", *Chemical Engineering Journal*, Vol. 234, pp. 140–148, 2013.

56. van Kampen, J., J. Boon, J. Vente and M. van Sint Annaland, "Sorption Enhanced Dimethyl Ether Synthesis under Industrially Relevant Conditions: Experimental Validation of Pressure Swing Regeneration", *Reaction Chemistry & Engineering*, Vol. 6, No. 2, pp. 244–257, 2021.

57. Skorikova, G., M. Saric, S. N. Sluijter, J. Van Kampen, C. Sánchez Martínez and J. Boon, "The Techno-economic Benefit of Sorption Enhancement: Evaluation of Sorption-enhanced Dimethyl Ether (DME) Synthesis for CO2 Utilisation", *Frontiers in Chemical Engineering*, Vol. 2, p. 22, 2020.

58. Liuzzi, D., C. Peinado, M. A. Pena, J. van Kampen, J. Boon and S. Rojas, "Increasing Dimethyl Ether Production from Biomass-derived Syngas via Sorption Enhanced Dimethyl Ether Synthesis", *Sustainable Energy & Fuels*, Vol. 4, No. 11, pp. 5674–5681, 2020.

59. De Falco, M., M. Capocelli and A. Basile, "Selective Membrane Application for the Industrial One-step DME Production Process Fed by CO2 Rich Streams: Modeling and Simulation", *International Journal of Hydrogen Energy*, Vol. 42, No. 10, pp. 6771–6786, 2017.

60. Wilson, M. E., N. Kota, Y. Kim, Y. Wang, D. B. Stolz, P. R. LeDuc and O. B. Ozdoganlar, "Fabrication of Circular Microfluidic Channels by Combining Mechanical Micromilling and Soft Lithography", *Lab on a Chip*, Vol. 11, No. 8, pp. 1550–1555, 2011.

61. Uriz, I., G. Arzamendi, E. Lopez, J. Llorca and L. Gandía, "Computational Fluid Dynamics Simulation of Ethanol Steam Reforming in Catalytic Wall Microchannels", *Chemical Engineering Journal*, Vol. 167, No. 2-3, pp. 603–609, 2011.

62. Hartvigsen, J. J., B. G. Nair, M. Wilson and A. Akash, "Catalytic Microchannel Re-

former", , Feb. 24 2015, uS Patent 8,961,625.

63. An, X., Y.-Z. Zuo, Q. Zhang, D.-z. Wang and J.-F. Wang, "Dimethyl Ether Synthesis from CO2 Hydrogenation on a CuO- ZnO- Al2O3- ZrO2/HZSM-5 Bifunctional Catalyst", *Industrial & Engineering Chemistry Research*, Vol. 47, No. 17, pp. 6547–6554, 2008.

64. Catizzone, E., G. Bonura, M. Migliori, F. Frusteri and G. Giordano, "CO2 Recycling to Dimethyl Ether: State-of-the-art and Perspectives", *Molecules*, Vol. 23, No. 1, p. 31, 2018.

65. Valle, B., A. G. Gayubo, A. Alonso, A. T. Aguayo and J. Bilbao, "Hydrothermally Stable HZSM-5 Zeolite Catalysts for the Transformation of Crude Bio-oil into Hydrocarbons", *Applied Catalysis B: Environmental*, Vol. 100, No. 1-2, pp. 318–327, 2010.

66. Graaf, G., E. Stamhuis and A. Beenackers, "Kinetics of Low-pressure Methanol Synthesis", *Chemical Engineering Science*, Vol. 43, No. 12, pp. 3185–3195, 1988.

67. Ji, G., G. Wang, K. Hooman, S. Bhatia and J. C. D. da COSTA, "Computational Fluid Dynamics Applied to High Temperature Hydrogen Separation Membranes", *Frontiers of Chemical Science and Engineering*, Vol. 6, No. 1, pp. 3–12, 2012.

68. Ozturk, N. F. and A. K. Avci, "Intensified Dimethyl Ether Production from Synthesis Gas with CO2", *Chemical Engineering Journal*, Vol. 370, pp. 885–896, 2019.

69. Engelbrecht, N., R. C. Everson, D. Bessarabov and G. Kolb, "Microchannel Reactor Heat-exchangers: A Review of Design Strategies for the Effective Thermal Coupling of Gas Phase Reactions", *Chemical Engineering and Processing-Process Intensification*, p. 108164, 2020.

70. Dongliang, W., M. Wenliang, Z. Huairong, L. Guixian, Y. Yong and L. Hongwei, "Green Hydrogen Coupling with CO2 Utilization of Coal-to-methanol for High Methanol Productivity and Low CO2 Emission", *Energy*, Vol. 231, p. 120970, 2021.